HHS Public Access

Author manuscript

Methods. Author manuscript; available in PMC 2019 September 15.

Published in final edited form as:

Methods. 2018 September 15; 148: 67–80. doi:10.1016/j.ymeth.2018.06.012.

Practical aspects of high-pressure NMR spectroscopy and its applications in protein biophysics and structural biology

José A. Caro and **A. Joshua Wand**

Johnson Research Foundation and Department of Biochemistry and Biophysics, University of Pennsylvania Perelman School of Medicine, Philadelphia, Pennsylvania 19104-6509

Abstract

Pressure and temperature are the two fundamental variables of thermodynamics. Temperature and chemical perturbation are central experimental tools for the exploration of macromolecular structure and dynamics. Though it has long been recognized that hydrostatic pressure offers a complementary and often unique view of macromolecular structure, stability and dynamics, it has not been employed nearly as much. For solution NMR applications the limited use of high-pressure is undoubtedly traced to difficulties of employing pressure in the context of modern multinuclear and multidimensional NMR. Limitations in pressure tolerant NMR sample cells have been overcome and enable detailed studies of macromolecular energy landscapes, hydration, dynamics and function. Here we review the practical considerations for studies of biological macromolecules at elevated pressure, with a particular emphasis on applications in protein biophysics and structural biology.

Keywords

high-pressure; solution NMR; structure determination; dynamics; thermodynamics

Introduction

Pressure is a fundamental thermodynamic variable that can provide a wealth of insight about protein stability, dynamics and function, much of which is often inaccessible through other perturbants such as temperature, pH and co-solutes. The structural and dynamic response of a protein molecule to pressure can vary significantly depending on local context. Furthermore, the influence of pressure is mediated by physical parameters that often provide complementary insight to that provided by chemical or temperature perturbation. The emergence of the ensemble as a framework for understanding the biophysical basis for

Contact Information: Professor A. J. Wand, 905 Stellar-Chance Laboratories, Department of Biochemistry & Biophysics, University of Pennsylvania Perelman School of Medicine, 422 Curie Blvd, Philadelphia, PA 19104-6059, telephone: 215-573-7288, wand@pennmedicine.upenn.edu.

Financial disclosure

AJW is a Member of Daedalus Innovations LLC, a manufacturer of high-pressure and reverse micelle NMR apparatus.

protein function strongly motivates the use of complementary methods that can provide distinct views of the energetics and character of the energy landscape of biomacromolecules. This article aims to discuss and familiarize the reader with the new capabilities in high-pressure NMR spectroscopy that have permitted re-examination of many fundamental yet unresolved issues in protein biophysics. The intent is to render the technique more accessible to the non-expert by describing the methodology and by providing a reference for common issues that have largely been overcome in the past decade.

Pressure thermodynamics

The molecular mechanisms of chemical and heat denaturation of proteins are relatively well established while those of pressure induced unfolding are not. Brandts and coworkers explained that the general principles used to describe the effects of heat on protein stability fail to describe how pressure denatures proteins [1]. The transfer of non-polar, model compound amino acids from a liquid hydrocarbon into water can be used to correlate the change in accessible surface area upon unfolding with the experimentally measured heat capacity [2]. In contrast, the observed ΔV of proteins cannot be simply predicted using transfer volumes of non-polar compounds and does not correlate with the change in surface area upon unfolding [3–7].

One advantage of using pressure is that it often enables *reversible* population of alternative or locally unfolded states that are often largely invisible to denaturants like heat or urea and potentially important to function and dysfunction of proteins [8–11]. As the conjugate variable of volume, variation of hydrostatic pressure can reveal information on the surface and internal hydration of proteins [12,13]. Pressure perturbation combined with solution NMR provides a site-resolved view, which is most often necessary to reach a comprehensive understanding of the biophysical properties determined by the highly heterogeneous internal structure of proteins. Illustrated here is how various phenomena accessible to solution NMR methods can be combined with high-pressure to gain decisive insight into the biophysical properties of proteins.

Early studies of the influence of pressure on proteins produced a rather complex and obscure view of protein thermodynamics. Very high-pressure (> 5 kbar) invariably produces protein denaturation while moderate pressures (~1 kbar) may even stabilize the native folded state, thereby increasing the temperature required for heat denaturation [14,15]. This behavior is a reflection of the fundamental parameters governing the response of protein solutions to pressure and temperature [14,16,17]. The difference in volume between the folded and unfolded states (ΔV) is the major determinant of the behavior of proteins under pressure. If the volume of the folded state is larger than that of the unfolded state then the ΔV will be negative. In this situation an increase in pressure will promote the unfolded state and lead to unfolding, according to the truncated Taylor expansion:

$$\Delta G(p,T) = \Delta G^\circ + \Delta V^\circ(p-p_0) + \frac{1}{2}\Delta\beta^\circ(p-p_0)^2 + \Delta\alpha^\circ(p-p_0)(T-T_0) \quad (1)$$
$$-\Delta C_P^\circ\left[T\left(ln\frac{T}{T_0}-1\right)+T_0\right] - \Delta S^\circ(T-T_0)$$

Here, ΔG° is the change in Gibbs free energy of the system with respect to the standard state of 1 bar (1 bar = 0.968 atm = 14.5 psi). The change in heat capacity ΔC_p° and the change in entropy ΔS° account for the temperature dependence while the pressure dependence is described by the change in volume (ΔV°) and the change in compressibility (Δβ°). The change in expansivity (Δα°) is dependent on both temperature and pressure.

Equation (1) serves as a two-state approximation and predicts, for parametric values appropriate to proteins, an ellipitical stability diagram whose contour separates the native state from the denatured state [14,18,19]. It is interesting to note that the temperature and the pressure denatured states are treated as equivalent, which is generally not true [9,10,14].

At constant temperature, equation (1) reduces to

$$\Delta G(p,T) = \Delta G^\circ + \Delta V^\circ(p-p_0) + \frac{1}{2}\Delta\beta^\circ(p-p_0)^2 \quad (2)$$

The change in isothermal compressibility of unfolding (Δβ°) represents the difference in the compressibility of the native and the unfolded states. There are conflicting experimental measurements of the magnitude of Δβ° [13,17,20–23]. Moreover, experimental limitations most often preclude accurate measurement of the higher order terms [24–27] of the Taylor expansion and are usually assumed to be negligible.

Structural origins of ΔV

Three main structural properties have been argued as being responsible for the negative ΔV of unfolding of proteins: 1) cavities present in the folded state that are eliminated upon unfolding; 2) changes in solvent density, including electrostriction, [28,29] arising from changes in protein solvation; and 3) the effects of pressure on the structure of bulk water [30]. Recent work with variants of Staphylococcal nuclease (SNase) indicate that relief of packing defects or voids within the native structure is a dominant contribution to the ΔV of unfolding [31]. Variants of SNase with larger cavities as observed by crystallography reported larger measured ΔV values. The extent of this correlation, the state of hydration of such artificial cavities, and their effect on the expansivity of the folded state remains to be fully explored [26,32,33]. Changes in solvent-exposed surface area, the physical basis for temperature and chemical denaturation, has also been used to explain the effects of pressure on proteins though no definitive correlation with ΔV has been observed [4,34]. It is also worth noting that, in cases where buried ionizable groups become charged upon unfolding, electrostriction can be significant [35–37]. Lastly, it has been proposed that pressure effects on the structure of bulk water can lead to the observed ΔV values. However, the low

pressures used in protein unfolding experiments, in particular the 5 bar used in pressure perturbation calorimetry (PPC) experiments, are unlikely to generate the type of change in the hydrogen bonding structure of water observed at pressures above 5 kbar [30]. Furthermore, ΔV values remain largely unchanged as a function of different solution compositions that shift the unfolding transition to various ranges of pressure, going as low as 500 bar [38].

Compressibility of the native state

Pressure perturbation below the unfolding transition of proteins has been widely used to explore the heterogeneous energy landscape of the native state. High-pressure crystallography and NMR spectroscopy have provided atomic resolution of the response of folded proteins to pressure. Crystallography has revealed subtle but relevant changes in structure, packing, and hydration patterns induced by pressure [12,39,40]. Solution NMR spectroscopy at room temperature has complemented, often recapitulated, and greatly extended these findings [41]. As detailed below, chemical shift analysis can reveal population redistributions between the native state and nearby alternative states or locally unfolded states [13,23,42]. Protein dynamics studies as a function of pressure have illustrated the large and heterogeneous response of side chains that accompany the more subtle structural changes [43,44]. Hydration dynamics studies have evaluated protein-water interactions in the confined space of reverse micelles, revealing increased and longer-lived protein-water interactions at high-pressure [13]. Combined with computational methods, NMR resonance intensity as a function of pressure have been used to guide biased simulations and visualize states along the folding pathway [11].

Apparatus

History

The advent of high-pressure NMR spectroscopy to study the chemical properties of water and organic solvent arose with an “autoclave” design of the NMR probe that involves placing the sample and the probe electronics under pressure within a self-contained metal housing [45]. Nearly 40 years later, Ballard et al. would use this approach to study the pressure unfolding of lysozyme [46,47], but the viability of the autoclave probe design in the context of modern triple resonance NMR was clearly limited. An obvious alternate strategy was to limit the pressurized region to the sample itself through the construction of a pressure tolerant NMR cell. In this approach the entire issue of placing the delicate components of a modern NMR probe under extreme pressure is avoided. Early approaches employed quartz capillaries that take advantage of the scaling of pressure tolerance with a reduced inner diameter [48,49]. Impressive pressures could be stably attained but the small active volume restricts the sample signal and prevents most experiments limited by high signal-to-noise requirements from being performed. Higher active volume tubes presented a technical challenge of joining the NMR sample cell to a high-pressure generator. One approach was to simply glue the tube to a pressure valve [50]. This proves somewhat unreliable at pressures approaching 1 kbar and therefore dangerous to the safe operation within the magnet. A more reliable strategy was introduced by Wand and coworkers [35,51] where a novel though

simple joining valve was utilized in a multi-stage sealing pressure flange (Figure 1). For the larger inner diameter tubes that are needed to maximize the sample in the active volume of the NMR probe the choice of material becomes critical. Single crystal edge-defined growth sapphire tubes were used initially [35,50,52]. Though having excellent tensile strength sapphire tubes are unfortunately brittle making their use in a high-pressure NMR context problematic. Subsequently Peterson and Wand [53] adopted advanced zirconia ceramics, which have exceptional tensile strength, are remarkably robust to shock, have generally excellent RF transmission characteristics, and can be machined to the high tolerances needed for high resolution NMR spectroscopy. Ceramic high-pressure NMR tubes have become commercially available and have helped to popularize the technique [41,54,55].

Current cell design and materials

Commercially available alumina-toughened zirconia tubes provide routine, stable and safe access to pressures up to 3 kbar and to a temperature range of −15 to 115 °C (Daedalus Innovations LLC of Aston, Pennsylvania). These tubes are compatible with standard 5 mm room temperature and cryogenically cooled probes. The 3 kbar rated tubes have an inner diameter of 2.8 mm and a working sample volume of about 225 μL, which allows for spectral quality near that of conventional tubes, and a total volume of 540 μL. Coupling to a pressure generator is achieved with a titanium or high-quality stainless steel valve that seals the tube to the pressure-transmitting tether. The tether is comprised of standard high-pressure stainless steel tubing and fittings. Multi-stage pressure sealing is used such that containment at lower pressures is maintained by an embedded o-ring and at higher pressures by a malleable washer. The pressure generating fluid can be water or organic solvent. Water is often preferable due to its low compressibility though this requires a high quality pressure generator. Pressurization using gases is strongly discouraged due to the potentially explosive kinetic energy that is stored. A layer of mineral oil acts an effective diffusion barrier between sample and pressurizing medium. A simple floating plastic plug is also useful in this context. The zirconia tubes are easy to handle and are remarkably sturdy. Nevertheless, some steps can be taken to mitigate tube failure [52,56]. The tube is matched to the valve by axial alignment as it is assembled. Once a seal is established, reversible pressure cycles between ambient pressure and 3 kbar can be performed multiple times without losing the seal or compromising NMR performance. In our hands, when handled with reasonable care, the tube can continuously hold maximum pressure literally for years and can repeat the pressurization cycle hundreds of times.

Pressure generators

There are many commercial suppliers of high-pressure generators. Simple manual operator generators of sufficient pressuring fluid volume and stability are available from Hi Pressure Equipment of Erie, Pennsylvania. Two suppliers of microprocessor - controlled high-pressure generators currently dominate the high-pressure NMR space. Daedalus Innovations LLC offers the Xtreme 60 pressure generator with a working volume of 6.7 mL and access to 4 kbar. This generator can be interfaced through the NMR console for remote control and programming of pressure profiles. Pressure Biosciences Inc (Medford, Massachusetts) offers the HUB880 barocycler with access to 6 kbar and is also capable of sophisticated pressure profiles and direct communication to the spectrometer. Pressure-jump applications have also

appeared with increasing sophistication though apparatus for the more advanced applications is custom-built [57–60]

Assembly and insertion

The high-pressure ceramic tube is matched to the cell once. In the process, a seat is crushed and molds to the surface of the tube and the cell. This seat prevents direct contact between the metallic cell and the tube. Unlike in lower pressure cells, this seat is not replaced. Subsequent assemblies will not achieve the quality of the match. As a result, the cell will experience minor (~100 bar/hr at 3 kbar) loss of pressure for which the generator will continually compensate without major consequences. The O-ring serves to prevent leaks at lower pressures and sits between the top of the NMR tube and the cell. To assemble it, a setup tool is used that houses the NMR tube in the cell (Figure 2). This tool is used to achieve radial alignment by rotating it while holding the cell static. The two titanium components of the cell are tightened using a torque wrench set to 130 in. lbs. Iterative cycles of tightening and rotations lead to optimal cell assembly. Once the cell is assembled and the tether is connected to the pump, it is important to test the seal by pressurizing the cell in a safety blast box, outside of the magnet. The cell should be then depressurized to ambient pressure and guided into the magnet, making sure the tether is secured, typically to the magnet and the ceiling. No abrupt motions should occur to the tether while the sample is in the magnet. Movement of the tether is typically prevented by using plastic tie-downs to secure the transmission line to the magnet fill ports.

Sample topics

pH Buffers

It is often overlooked that changes in pressure can result in electrostriction effects in buffers that will significantly affect the pH [16]. This is particularly true for anionic buffers like phosphate and MES, which display large ΔV values of −20.3 and +13.5 mL/mol, respectively, over 1 kbar. On the other hand, cationic and zwitterionic buffers have relatively low ΔV values [16,61–66]. The pressure sensitivity of pH can be averted using appropriate mixtures of buffer components that result in balancing contributions to ΔV and yield no or minimal net response in pH to pressure (Table 1 and Figure 3) [67].

Viscosity

NMR spectroscopy is highly sensitive to the tumbling rates of macromolecules, making the viscosity of sample solutions an important factor. Fortuitously, in the pressure range accessible to standard NMR experiments and at room temperature, the viscosity of water is largely unaffected, though buffers will modify the structure of water in various ways. The viscosity of many organic solvents and water have been catalogued by Bridgman and others. A highly informative server is available at the National Institute of Standards and Technology (NIST) (https://webbook.nist.gov/chemistry/fluid/).

Chemical shift referencing

The influence of pressure on protein structure is often gleaned from analysis of changes in chemical shifts such as the amide ^{15}N-^{1}H correlation. As with temperature, the chemical

shift of water changes with pressure and cannot be used as quantitative reference. An internal standard such as tetramethylsilane (TMS) offers a much better internal chemical shift reference. Though modestly pressure sensitive, explicit calibration [10] yields the following equation for use of TMS over the full pressure range available with current apparatus

$$\delta(p,T) = 7.866 ppm - 1.612 \cdot 10^{-4} \frac{ppm}{bar} \cdot p - 1.025 \cdot 10^{-2} \frac{ppm}{K} \cdot T + 5.945 \cdot 10^{-7} \frac{ppm}{bar \cdot K} \cdot p \cdot T \quad (3)$$

Analysis

The chemical shift is the NMR observable most often used to monitor the effects of pressure on the structure of proteins. The physical origins of changes in chemical shifts due to pressure of NMR-detected nuclei has been studied at length, and involve compression of hydrogen bonds, covalent bonds, distortion of dihedral angles, and alteration of side chain orientations [10,73–78]. Studies of model peptides detail the effects of pressure on chemical shifts, highlighting the need to distinguish them from the responses specific to proteins 79–81]. Empirically, changes in chemical shifts due to pressure can be fit to a 2nd order Taylor expansion:

$$\delta(p) = \delta_0(p_0) + B_1(p - p_0) + B_2(p - p_0)^2 \quad (4)$$

Here, the pressure dependence of δ is defined by its value at atmospheric pressure p_0 and the linear and quadratic coefficients B_1 and B_2 (see [11,82,83]). It is possible to interpret a large quadratic component in the context of alternative states. Following Le Châtelier's principle, pressure will favor population of states with lower volumes, including a third, alternative state in fast exchange with the native resonance. Increased population of such a third state will likely result in a non-linear δ (p).

Erlach et al. extended the formalism of equation (4) to obtain thermodynamic information [84]. By assuming a two-state process, they define an exact partition function that confers thermodynamic meaning to the coefficients B_1 and B_2. The ratio of B_2 over B_1 can then be defined in terms of ΔG, ΔV and Δ β as follows

$$\frac{B_2}{B_1} = -\frac{\Delta\beta(p_0)}{\Delta V(p_0)} - \frac{\Delta V(p_0)}{RT_0} \tanh\left(\frac{\Delta G^\circ}{2RT_0}\right) \quad (5)$$

In the limit of ΔG << 2RT, the second term vanishes and one is left with a ratio of the change in compressibility and volume between the two substates. In the case of larger energy gaps between two substates, the limit of ΔG>>2RT simplifies the second term and isolates ΔV, which can then be determined as a function of temperature. It is not, however,

obvious as to how to extract physical meaning from the ratio Δβ/ΔV. Peptide studies and modeling suggest a dependence of the Δβ/ΔV ratio on the hydrogen- bonding network [80].

It is important to remember that chemical shifts are determined by the electronic environment of the probed nucleus and not by the thermodynamic properties of the native state. For example, alternative states in intermediate exchange would be undetectable, chemical shifts of different probes can report on different physical phenomena, and the magnitude of the coefficients in δ(p) do not need to correlate with the thermodynamic properties of the exchanging states, including Δβ Nevertheless, chemical shift changes can also report on the physical contributors to the compressibility of proteins such as the existence of multiple states in the folded ensemble that are sensitive to pressure, including locally unfolded states, and on the broadening or narrowing of the energy well of a “single” (the native) state. In particular, it has been found that proteins in which large cavities were engineered yield larger B_2 values, suggestive of a wider ensemble of accessible conformations [11,23,32,42,85].

Examples

Chemical shift perturbation

As explained above, the heterogeneous and reversible response of proteins to pressure can be monitored in a site-specific manner using chemical shifts [11,13,42,86,87]. By collecting spectra at a series of pressures, one can track the chemical shifts as they respond to pressure. For example, Roche et al. performed a systematic study of the effect of engineered cavities on the amide chemical shifts of SNase [38] (Figure 4). For each variant studied, a subset of chemical shift traces showed non-linearity. Mapping of the second-order B_2 values onto the structure highlighted the poorly packed region of the protein where the engineered cavity was introduced. The site-specific response to pressure observed here for proteins with artificial cavities offers insight into the potential mechanisms whereby proteins can undergo excursions to non-native states and the physical determinants of complex energy landscapes.

Resonance intensity analysis

The unfolding transition of proteins can be monitored using resonance intensities as a function of pressure. A pressure series that exceeds the mid-point of unfolding of the protein can be used to monitor site-specific unfolding profiles and fit to a thermodynamic model to extract ΔV values. This approach is typically limited to native state reporters, since resonances of unfolded proteins are often overlapped and difficult to assign. Louis & Roche overcame this challenge by assigning the unfolded state of a multidrug resistant variant of HIV-1 protease and determined a much more homogeneous transition for denatured resonances (Figure 5). This is consistent with fast-to-intermediate timescale exchange within the native state but not the unfolded state. To explore the structural origins of such conformational fluctuations, Roche et al. used pressure to study the unfolding behavior of SNase and a set of its variants with artificial cavities [31]. Both the magnitude and distribution of the ΔV values observed were indicative of a central role of cavities in determining the pressure sensitivity and folding cooperativity of proteins (Figure 6). Following Le Châtelier’s principle, Kitahara and coworkers also explored the role of cavities

by monitoring methyl resonances of the L99A variant of T4 lysozyme L99A as a function of pressure [42]. The experiment highlighted a markedly different behavior in peak intensity between methyls directly adjacent to the engineered cavity and the rest of the methyls (Figure 7). The work starkly illustrates the non-cooperative behavior imparted by the artificial cavity on this protein. Though there was some disagreement on the interpretation of some the pressure sensitivity seen in T4 lysozyme, these works illustrate the detailed structural and energetic information that can be gleaned from high-pressure NMR spectroscopy [13,85,86]. Resonance intensities can also be used to monitor the effect of binding on the thermodynamic stability and cooperative nature of multimeric protein complexes. In another recent example, Fuglestad et al. use high-pressure NMR spectroscopy to study the homodimeric regulatory domain of the lac repressor [23]. They find that high-pressure induces multiple structural transitions, with a major cooperative subglobal unfolding event that nevertheless maintains the dimeric complex.

Structural determination

Detailed and comprehensive structural analysis of proteins under high hydrostatic pressure is relatively sparse. The structure of a intermediate state of ubiquitin that is populated at high-pressure has been characterized in detail using classical NOE-based distance and torsion angle restraints. This work clearly demonstrates that the usual experimental restraints can be obtained in this context. More recently, partial alignment media have been evaluated for tolerance to high-pressure and many have been found to be remarkably robust even up to 2.5 kbar [91–93].

Protein dynamics

High-pressure NMR spectroscopy has also been implemented to study the dynamics of proteins at various timescales. Classical spin relaxation experiments probe the ps-ns timescale dynamics of proteins. The Lipari-Szabo squared generalized order parameter O^2 (or S^2 in the original formalism) has recently been shown to be intimately related to the entropy change of protein-ligand interactions. A limited number of studies exist on the pressure dependence of O^2, most of which focus on the backbone amide relaxation properties. It is well known that at ambient pressure (and for structured proteins) a very narrow distribution of O^2 values between 0.80 and 0.95 is typical for amide N-H bond vectors in well-structured regions of the protein. These values are near the theoretical upper limit of 1 for O^2, and generally change little in response to thermodynamic perturbations such as pressure and even binding events. In contrast, motions of the symmetry axis of methyl groups (O^2axis) span nearly the full range of accessible motion and are generally more sensitive to both physical, chemical and biological perturbation (e.g. ligand binding) than the polypeptide backbone. The structural properties that determine O^2axis values remain largely unknown (Figure 8). In a unique study of its kind, Fu et al. determined the pressure dependence of methyl O^2 values in ubiquitin (Figure 9) [43]. Several key findings resulted that promote investigation along these lines in other systems. First, a general increase was observed in the average O^2 value of methyl-bearing side chains with increased pressure, illustrating an effect of compression of the native state. Second, despite a highly heterogeneous response, spatial clustering of side chains with similar pressure dependence were observed, highlighting the existence of regions with differing compressibility.

Importantly, this behavior indicates limited coupling of side chain motion. Finally, a relationship was found that indicates that methyls with lower O^2 values (more mobile) are also the most sensitive to pressure, which likely warrants additional studies of the relationship between side chain motion and volume.

With respect to aromatic side chains, pioneering work by Wagner using a high-pressure glass capillary probed the activation volume of aromatic ring flips in BPTI. Line shape analysis of ^1H resonances enabled an estimation of $\Delta V^\dagger$ for aromatic ring flips of about 30 mL/mol. Similar studies that included temperature variation were later carried out by Li et al. and Hattori et al. using a quartz capillary tube resistant to pressures of up to 2 kbar. A more recent study by Kasinath et al. involved specific labeling of aromatic of dynamics of aromatic side chains in ubiquitin as a function of temperature and pressure. At temperatures below 300 K, the O^2 values of Phe and Tyr side chains are >0.7 and essentially insensitive to pressure (Figure 10). A transition is observed at about 310 K, which was interpreted as thermal activation of ring rotation into the timescale accessible by classical NMR autorelaxation (i.e. faster than the overall tumbling of the protein). This motion is sensitive to pressure and yields $\Delta O^2/\Delta P$ values comparable to those of ubiquitin's methyl-bearing side chains (~4 $kbar^{-1}$). Overall, this suggests that the interior of the protein is much more liquid-like than perhaps appreciated and emphasizes the observation by Akke and coworkers that the slow ring flipping with a high activation volume seen in early studies represents the minority of aromatic amino acid side chains [103].

The work on aromatic ring dynamics exemplifies the importance of probing motions in proteins on many timescales and employing perturbations such as pressure to reveal the physical character of the underlying motion. Relaxation dispersion experiments are ideally suited to high-pressure NMR spectroscopy, where small, reversible perturbations can shift the equilibrium of substates in intermediate- and slow-exchange along the folding pathway. Korzhnev et al. studied the intermediate timescale dynamics of cyt b_{562} under conditions in which the protein is marginally stable. Under remarkably low pressures (270 bar) significant relaxation dispersion profiles were observed for 60% of amides in the protein (Figure 11). The dispersion was attributed to exchange between folded and unfolded states of the protein. Pressure increased the rate of exchange. Interpretation in the context of a 2-state folding reaction yielded folding and unfolding rates, as well as ΔV and $\Delta\beta$ values of the reaction. The kinetics of exchange directly provided access to the thermodynamics of the transition state yielding for $\Delta V^\dagger$ and $\Delta\beta^\dagger$ values of unfolding. Similarly, Bezsonova et al. implemented CPMG-type relaxation dispersion as a function of pressure to decompose the multistep folding pathway of an SH3 domain. Another relaxation dispersion study of a variant of the same SH3 domain exploited the full 2.5 kbar pressure range to collect an extensive dataset [27]. The thermodynamic values obtained are consistent with previously published values. The authors remark that, despite the wealth of data obtained, the choice of thermodynamic model remains a challenge and results in some variability of the parameters obtained.

Unlike chemical or heat perturbation, pressure perturbation typically results in a readily discernable and heterogeneous response of the protein, which is determined in part by the distribution of cavities [11,31,42,106,107]. The ability of pressure to locally destabilize the protein fold often results in the population of alternative states and of species with locally

unfolded regions that can be functionally relevant or play an important role in aggregate or amyloid nucleation (15, 18, 34, 35). Hydrogen/deuterium exchange (HX) monitored by NMR spectroscopy can directly probe the thermodynamic stability of subglobal domains, or foldons, and local unfolding events. HX is most often monitored by serial acquisition of two-dimensional ^{15}N-correlated spectra. When better resolution is required, three-dimensional radially sampled HNCO spectra can also be used. The latter, termed AMORE-HX, employs radial sampling and true two-dimensional Fourier transforms and achieves excellent time resolution and avoids the artifacts and non-linearity of non-uniform sampling for low signal-to-noise signals [109.

When combined with pressure, it is possible to extract the ΔV values of transitions detected by HX. Fuentes & Wand used high-pressure HX to identify three regions in apocytochrome b_{562} with distinct pressure sensitivities, including one subdomain with a positive volume change with pressure that indicates the presence of a highly mispacked open state (Figure 12) (36). The ΔG values extracted from these experiments agree well with those obtained from HX as a function of chemical denaturant (Gdn HCl). Some precautions have to be taken to correct for pressure effects on the pK_a of water and the rates of hydrogen exchange (37). Fuentes & Wand note that the corrections are typically small and on the order of a factor of 2. The exchange rate corrections as a function of temperature and pressure have been summarized by the authors and yield the following equation (36)

$$k(p) = k_0(p_0)exp\left[-\frac{(p-p_0)}{RT}\Delta V^{\dagger}\right] \quad (6)$$

Here, one can use the following activation volumes to correct for the acid, base, and water hydrogen exchange rate constants: $\Delta V^{\dagger}_{H^+}$ = +1.7 mL/mol, $\Delta V^{\dagger}_{OH^-}$ = +11 mL/mol, $\Delta V^{\dagger}_{H_2O}$ = −9 mL/mol. As to the pressure dependence of the pK_a of water, the following empirical relationship has been determined

$$pK_w(T,p) - pK_w(T,p_0) = -\frac{p\Delta V_{K_W}}{2.303RT(1+bp)} \quad (7)$$

The constant b is 9.2×10^{-5} bar^{-1} and one can use an ionization volume of water ΔV_{KW} of −22.1 mL/mol.

Protein hydration

Perhaps the most significant question high-pressure NMR spectroscopy will address is the role of water in determining protein structure and function. The structural determinants of ΔV are thought to involve the differential solvation of internal cavities, relative to hydration of the protein surface, and of ionizable and non-ionizable residues upon unfolding [11]. Perturbation by pressure directly probes the role of solvent in determining the stability and volume of proteins, and can provide novel insight into the role of water in catalytic sites of enzymes, refine the contribution from specific and allosteric hydration to protein binding

reactions, and illuminate the role of solvent in determining the dynamics of proteins. The ability to directly monitor protein-water interactions through the nuclear Overhauser effect (NOE) as proposed some time ago by Wüthrich and coworkers offers unique access to hydration dynamics in the ns timescale. Coupled with reverse micelle encapsulation technology [111,112], magnetization transfer between water protons and amide hydrogens of a protein can be used to characterize the dynamics of hydration water [113,114]. A recent application investigated the surface and internal hydration of the L99A cavity mutant of T4 lysozyme [13]. The entry of water into the largely hydrophobic cavity increased with applied hydrostatic pressure and allowed the thermodynamics of hydration to be established (Figure 13).

Kinetics

Time-resolved kinetics measurements have provided insight into the folding landscape of proteins and, coupled with simulation, have helped to visualize sub-ms folding transitions. Sub-ms pressure-jump kinetics have been shown to provide complementary information and can be used to benchmark molecular dynamics engine force fields [115,116]. Pressure-jump NMR spectroscopy has the ability to characterize the kinetics of folding site-specifically and with many reporters, but it remains a challenge to access fast timescales. To overcome this, Roche et al. took advantage of the large and positive activation volume of unfolding of SNase and its variants with artificial cavities and chose to work at high-pressures to slow the reaction down [11]. Pressure jumps of 200 bar were followed using SOFAST-HSQC measurements over 24 hours. The wealth of information provided by over 100 NH reporters described a markedly different and much more complete picture of the folding behavior of SNase from that obtained from the fluorescence of Trp-140, though the transition state volumes recorded for Trp-140 itself matched those measured by fluorescence. Another approach incorporates jumps of 800 bar in less than 30 ms into the NMR pulse sequence [59]. This allows for unprecedented monitoring of protein transitions at atomic resolution and in real time.

The introduction of large pressure perturbations within the NMR pulse sequence allows encoding of spectral properties of different thermodynamic states [59]. To implement this approach a custom microprocessor-controlled pressure jump was interfaced to the spectrometer and able to introduce fast, strong pressure changes in the pulse sequences [59]. Repetitive pressure changes of 800 bar in less than 30 ms were achievable. Kalbitzer and coworkers [59] describe two general experiments enabled by this apparatus: pressure perturbation transient state spectroscopy (PPTSS) and the pressure perturbation state correlation spectroscopy (PPSCS) [59]. PPTSS can be used to measure the rate constants and the activation energies and activation volumes for the transition between different conformational states. PPSCS spectroscopy correlates the NMR parameters of different pressure-induced states of the system, thus allowing the measurement of properties of a given pressure induced state. In a very recent example, Bax and coworkers have greatly advanced the pressure-jump capability and reached 3–5 ms pressure transition speeds with good reproducibility and long-term stability [60,117]. This custom pressure jump NMR apparatus is capable of switching between 2.5 kbar and atmospheric pressure hundreds of times and can be fully integrated into the NMR pulse sequence. This setup was used to study

a variant of ubiquitin with artificial cavities and identified two parallel and competing folding pathways, as well as oligomeric off-pathway intermediates at higher protein concentrations.

Conclusion

The advent of simplified, commercially available high-pressure apparatus for high-resolution solution NMR spectroscopy has enabled a plethora of new and exciting areas of research. Here we have provided a general outline for properly and safely performing NMR experiments under pressure. The implementation of high pressure in the context of advanced heteronuclear NMR of biological macromolecules is now straightforward. We have strived to point the reader to notable of applications of high-pressure NMR in the characterization of the physical properties of proteins. The quantitative interpretation of high-pressure perturbation allows for deep insight into the underlying physical properties that is often not otherwise available.

Acknowledgments

High-pressure NMR work in the Wand laboratory has been supported by the NIH, the NSF and the Mathers Foundation.

Bibliography

[1]. Brandts JF, Oliveira RJ, and Westort C Thermodynamics of protein denaturation. Effect of pressure on the denaturation of ribonuclease A", Biochemistry 9 (1970) 1038–1047. [PubMed: 5417389]

[2]. Kauzmann W Some factors in the interpretation of protein denaturation, Adv. Protein Chem. 14 (1959) 1–63. [PubMed: 14404936]

[3]. Zipp A and Kauzmann W Pressure denaturation of metmyoglobin, Biochemistry 12 (1973) 4217–4228. [PubMed: 4795687]

[4]. Frye KJ, Perman CS, and Royer CA Testing the correlation between ΔA and ΔV of protein unfolding using m value mutants of staphylococcal nuclease., Biochemistry 35 (1996) 10234–10239. [PubMed: 8756489]

[5]. Kauzmann W Thermodynamics of unfolding, Nature 325 (1987) 763–764.

[6]. Baldwin RL Temperature dependence of the hydrophobic interaction in protein folding., Proc. Natl. Acad. Sci. USA 83 (1986) 8069–8072. [PubMed: 3464944]

[7]. de Oliveira GA and Silva JL A hypothesis to reconcile the physical and chemical unfolding of proteins, Proc Natl Acad Sci U S A 112 (2015) E2775–2784. [PubMed: 25964355]

[8]. Ohmae E, Murakami C, Tate S, Gekko K, Hata K, Akasaka K, and Kato C Pressure dependence of activity and stability of dihydrofolate reductases of the deep-sea bacterium Moritella profunda and Escherichia coli, Biochim. Biophys. Acta 1824 (2012) 511–519. [PubMed: 22266402]

[9]. Zhang J, Peng X, Jonas A, and Jonas J NMR study of the cold, heat, and pressure unfolding of ribonuclease A., Biochemistry 34 (1995) 8631–8641. [PubMed: 7612603]

[10]. Vajpai N, Nisius L, Wiktor M, and Grzesiek S High-pressure NMR reveals close similarity between cold and alcohol protein denaturation in ubiquitin, Proc. Natl. Acad. Sci. USA 110 (2013) E368–E376. [PubMed: 23284170]

[11]. Roche J, Caro JA, Dellarole M, Guca E, Royer CA, Garcia-Moreno BE, Garcia AE, and Roumestand C Structural, energetic, and dynamic responses of the native state ensemble of staphylococcal nuclease to cavity-creating mutations, Proteins 81 (2013) 1069–1080. [PubMed: 23239146]

[12]. Collins MD, Hummer G, Quillin ML, Matthews BW, and Gruner SM Cooperative water filling of a nonpolar protein cavity observed by high-pressure crystallography and simulation, Proc. Natl. Acad. Sci. USA 102 (2005) 16668–16671. [PubMed: 16269539]

[13]. Nucci NV, Fuglestad B, Athanasoula EA, and Wand AJ Role of cavities and hydration in the pressure unfolding of T4 lysozyme, Proc. Natl. Acad. Sci. USA 111 (2014) 13846–13851. [PubMed: 25201963]

[14]. Hawley SA Reversible pressure-temperature denaturation of chymotrypsinogen, Biochemistry 10 (1971) 2436–2442. [PubMed: 5557794]

[15]. Johnson FH and Campbell DH Pressure and protein denaturation, J. Biol. Chem 163 (1946) 689–698. [PubMed: 20985641]

[16]. Neuman RC, Kauzmann W, and Zipp A Pressure-dependence of weak acid ionizastion in aqueous buffers., J. Phys. Chem 77 (1973) 2687–2691.

[17]. Heremans K and Smeller L Protein structure and dynamics at high pressure., Biochim. Biophys. Acta 1386 (1998) 353–370. [PubMed: 9733996]

[18]. Lesch H, Stadlbauer H, Friedrich J, and Vanderkooi JM Stability diagram and unfolding of a modified cytochrome c: What happens in the transformation regime?, Biophys. J 82 (2002) 1644–1653. [PubMed: 11867476]

[19]. Lesch H, Hecht C, and Friedrich J Protein phase diagrams: The physics behind their elliptic shape, J. Chem. Phys 121 (2004) 12671–12675. [PubMed: 15606293]

[20]. Seemann H, Winter R, and Royer CA Volume, expansivity and isothermal compressibility changes associated with temperature and pressure unfolding of Staphylococcal nuclease, J. Mol. Biol 307 (2001) 1091–1102. [PubMed: 11286558]

[21]. Prehoda KE, Mooberry ES, and Markley JL Pressure denaturation of proteins: evaluation of compressibility effects., Biochemistry 37 (1998) 5785–5790. [PubMed: 9558311]

[22]. Lassalle MW, Yamada H, and Akasaka K The pressure-temperature free energy-landscape of staphylococcal nuclease monitored by (1)H NMR, J. Mol. Biol 298 (2000) 293–302. [PubMed: 10764598]

[23]. Fuglestad B, Stetz MA, Belnavis Z, and Wand AJ Solution NMR investigation of the response of the lactose repressor core domain dimer to hydrostatic pressure, Biophys. Chem 231 (2017) 39–44. [PubMed: 28249763]

[24]. Smeller L Pressure-temperature phase diagrams of biomolecules., Biochemi. Biophys. Acta 1595 (2002) 11–29.

[25]. Chalikian TV and Macgregor RB, Jr Origins of pressure-induced protein transitions., J. Mol. Biol 394 (2009) 834–842. [PubMed: 19837081]

[26]. Lin L-N, Brandts JF, Brandts JM, and Plotnikov V Determination of the volumetric properties of proteins and other solutes using pressure perturbation calorimetry, Anal. Biochem 302 (2002) 144–160. [PubMed: 11846388]

[27]. Tugarinov V, Libich DS, Meyer V, Roche J, and Clore GM The energetics of a three-state protein folding system probed by high-pressure relaxation dispersion NMR spectroscopy, Angew Chem Int Ed Engl 54 (2015) 11157–11161. [PubMed: 26352026]

[28]. Ben-Naim A and Marcus Y Solvation thermodynamics of nonionic solutes, J. Chem. Phys 81 (1984) 2016.

[29]. Marcus Y A simple empirical model describing the thermodynamics of hydration of ions of widely varying charges, sizes, and shapes, Biophys. Chem 51 (1994) 111–117.

[30]. Jonas J Nuclear magnetic resonance at high pressure, Science 216 (1982) 1179–1184. [PubMed: 17830561]

[31]. Roche J, Caro JA, Norberto DR, Barthe P, Roumestand C, Schlessman JL, Garcia AE, Garcia-Moreno BE, and Royer CA Cavities determine the pressure unfolding of proteins, Proc. Natl. Acad. Sci. USA 109 (2012) 6945–6950. [PubMed: 22496593]

[32]. Dellarole M, Kobayashi K, Rouget J-B, Caro JA, Roche J, Islam MM, García-Moreno EB, Kuroda Y, and Royer CA Probing the physical determinants of thermal expansion of folded proteins., J. Phys. Chem. B 117 (2013) 12742–12749. [PubMed: 23646824]

[33]. Tsamaloukas AD, Pyzocha NK, and Makhatadze GI Pressure perturbation calorimetry of unfolded proteins, J. Phys. Chem. B (2010) 16166–16170. [PubMed: 20831285]

[34]. Rouget J-B, Aksel T, Roche J, Saldana J-L, Garcia AE, Barrick D, and Royer CA Size and sequence and the volume change of protein folding., J. Am. Chem. Soc 133 (2011) 6020–6027. [PubMed: 21446709]

[35]. Urbauer JL, Ehrhardt MR, Bieber RJ, Flynn PF, and Wand AJ High-resolution triple-resonance NMR spectroscopy of a novel calmodulin-peptide complex at kilobar pressures, J. Am. Chem. Soc 118 (1996) 11329–11330.

[36]. Brun L, Isom DG, Velu P, García-Moreno EB, and Royer CA Hydration of the folding transition state ensemble of a protein, Biochemistry 45 (2006) 3473–3480. [PubMed: 16533028]

[37]. Kitahara R, Hata K, Maeno A, Akasaka K, Chimenti MS, García-Moreno EB, Schroer M.a., Jeworrek C, Tolan M, Winter R, Roche J, Roumestand C, Montet de Guillen K, and Royer CA Structural plasticity of staphylococcal nuclease probed by perturbation with pressure and pH, Proteins 79 (2011) 1293–1305. [PubMed: 21254234]

[38]. Roche J, Dellarole M, Caro JA, Guca E, Norberto DR, Yang Y, Garcia AE, Roumestand C, Garcia-Moreno B, and Royer CA Remodeling of the folding free energy landscape of staphylococcal nuclease by cavity-creating mutations, Biochemistry 51 (2012) 9535–9546. [PubMed: 23116341]

[39]. Nagae T, Kawamura T, Chavas LM, Niwa K, Hasegawa M, Kato C, and Watanabe N High-pressure-induced water penetration into 3-isopropylmalate dehydrogenase, Acta Crystallogr. D Biol. Crystallogr 6 (2012) 300–309.

[40]. Kundrot CE and Richards FM Effect of hydrostatic pressure on the solvent in crystals of hen egg-white lysozyme., J. Mol. Biol 200 (1988) 401–410. [PubMed: 3373535]

[41]. Roche J, Royer CA, and Roumestand C Monitoring protein folding through high pressure NMR spectroscopy, Prog. Nucl. Magn. Reson. Spectrosc 102–103 (2017) 15–31.

[42]. Maeno A, Sindhikara D, Hirata F, Otten R, Dahlquist FW, Yokoyama S, Akasaka K, Mulder FA, and Kitahara R Cavity as a source of conformational fluctuation and high-energy state: high-pressure NMR study of a cavity-enlarged mutant of T4 lysozyme, Biophys. J 108 (2015) 133–145. [PubMed: 25564860]

[43]. Fu Y, Kasinath V, Moorman VR, Nucci NV, Hilser VJ, and Wand AJ Coupled motion in proteins revealed by pressure perturbation, J. Am. Chem. Soc 134 (2012) 8543–8550. [PubMed: 22452540]

[44]. Kasinath V, Fu Y, Sharp KA, and Wand AJ A sharp thermal transition of fast aromatic-ring dynamics in ubiquitin, Angew. Chem. Int. Ed. Engl 54 (2015) 102–107. [PubMed: 25476230]

[45]. Benedek GB and Purcell EM Nuclear magnetic resonance in liquids under high pressure, J. Chem. Phys 22 (1954) 2003.

[46]. Ballard L, Reiner C, and Jonas J High-resolution NMR probe for experiments at high pressures, J. Magn. Reson. Ser A 123 (1996) 81–86. [PubMed: 8980066]

[47]. Jonas J, Ballard L, and Nash D High-resolution, high-pressure NMR studies of proteins, Biophys. J 75 (1998) 445–452. [PubMed: 9649405]

[48]. Yamada H Pressure-resisting glass cell for high pressure, high resolution NMR measurement, Rev. Sci. Instrum 45 (1974) 640–642.

[49]. Yamada H, Nishikawa K, Honda M, Shimura T, Akasaka K, and Tabayashi K Pressure-resisting cell for high-pressure, high-resolution nuclear magnetic resonance measurements at very high magnetic fields, Rev. Sci. Instrum 72 (2001) 1463.

[50]. Roe DC Sapphire NMR tube for high-resolution studies at elevated pressure., J. Magn. Reson 63 (1985) 388–391.

[51]. Wand AJ, Earhardt MR, and Urbauer JL, Apparatus and method for high pressure NMR spectroscopy U.S. Patent, Editor. 2002, The Research Foundation of State University of New York (Amherst, NY) USA.

[52]. Arnold MR, Kalbitzer HR, and Kremer W High-sensitivity sapphire cells for high pressure NMR spectroscopy on proteins, J. Magn. Reson 161 (2003) 127–131. [PubMed: 12713961]

[53]. Peterson RW and Wand AJ Self contained high pressure cell, apparatus and procedure for the preparation of encapsulated proteins dissolved in low viscosity fluids for NMR spectroscopy, Rev. Sci. Instrum 76 (2005) 1–7.

[54]. Akasaka K, Protein studies by high-pressure NMR, in Experimental approaches of NMR spectroscopy, T.n.m.r.s.o. Japan, Editor. 2017, Springer p. 3–36.

[55]. Akasaka K, High pressure NMR spectroscopy, in High pressure bioscience K Akasaka and H. Matsuki, Editors. 2015, Springer.

[56]. Erlach MB, Munte CE, Kremer W, Hartl R, Rochelt D, Niesner D, and Kalbitzer HR Ceramic cells for high pressure NMR spectroscopy of proteins, J. Magn. Reson 204 (2010) 196–199. [PubMed: 20359919]

[57]. Kitahara R, Royer C, Yamada H, Boyer M, Saldana J-L, Akasaka K, and Roumestand C Equilibrium and pressure-jump relaxation studies of the conformational transitions of P13MTCP1, J. Mol. Biol 320 (2002) 609–628. [PubMed: 12096913]

[58]. Kamatari YO, Yokoyama S, Tachibana H, and Akasaka K Pressure-jump NMR study of dissociation and association of amyloid protofibrils, J. Mol. Biol 349 (2005) 916–921. [PubMed: 15907935]

[59]. Kremer W, Arnold M, Munte CE, Hartl R, Erlach MB, Koehler J, Meier A, and Kalbitzer HR Pulsed pressure perturbations, an extra dimension in NMR spectroscopy of proteins, J. Am. Chem. Soc 133 (2011) 13646–13651. [PubMed: 21774550]

[60]. Charlier C, Alderson TR, Courtney JM, Ying J, Anfinrud P, and Bax A Study of protein folding under native conditions by rapidly switching the hydrostatic pressure inside an NMR sample cell, Proc. Natl. Acad. Sci. USA (2018)

[61]. Hayert M, Pierre-Cornet J-M, and Gervais P A simple method for measuring the pH of acid solutions under high pressure, J. Phys. Chem. A 103 (1999) 1785–1789.

[62]. Surdo AL, Bernstrom K, Jonsson CA, and Millero FJ Molal volume and adiabatic compressibility of aqueous phosphate solutions at 25 C, J. Phys. Chem 83 (1979) 1255–1262.

[63]. Orlien V, Olsen K, and Skibsted LH In situ measurements of pH changes in beta-lactoglobulin solutions under high hydrostatic pressure, J. Agric. Food Chem 55 (2007) 4422–4428. [PubMed: 17461592]

[64]. Salerno M, Ajimo JJ, Dudley JA, Binzel K, and Urayama P Characterization of dual-wavelength seminaphthofluorescein and seminapthorhodafluor dyes for pH sensing under high hydrostatic pressures, Anal. Biochem 362 (2007) 258–267. [PubMed: 17274941]

[65]. Kitamura Y and Itoh T Reaction volume of protonic ionization for buffering agents. Prediction of pressure dependence of pH and pOH, J. Solution Chem 16 (1987) 715–725.

[66]. Tsuda M, Shirotani I, Minomura S, and Terayama Y The effect of pressure on the dissociation of weak acids in aqueous buffers, Bull. Chem. Soc. Japan 49 (1976) 2952–2955.

[67]. Quinlan RJ and Reinhart GD Baroresistant buffer mixtures for biochemical analyses, Anal. Biochem 341 (2005) 69–76. [PubMed: 15866529]

[68]. Bridgman PW The viscosity of liquids under pressure, Proc. Natl. Acad. Sci. USA 11 (1925) 603–606. [PubMed: 16587047]

[69]. Bett KE and Cappi JB Effect of pressure on the viscosity of water, Nature 207 (1965) 620–621.

[70]. Horne RA and Johnson DS The viscosity of water under pressure, J. Phys. Chem 70 (1966) 2182–2190.

[71]. Akasaka K Highly fluctuating protein structures revealed by variable-pressure nuclear magnetic resonance, Biochemistry 42 (2003) 10875–10885. [PubMed: 12974621]

[72]. Akasaka K Exploring the entire conformational space of proteins by high-pressure NMR, Pure Appl.Chem 75 (2003) 927–936.

[73]. Akasaka K and Li H Low-lying excited states of proteins revealed from nonlinear pressure shifts in 1H and 15N NMR, Biochemistry 40 (2001) 8665– 8671. [PubMed: 11467925]

[74]. Nisius L and Grzesiek S Key stabilizing elements of protein structure identified through pressure and temperature perturbation of its hydrogen bond network, Nat. Chem 4 (2012) 711–717. [PubMed: 22914191]

[75]. Wilton DJ, Kitahara R, Akasaka K, Pandya MJ, and Williamson MP Pressure-dependent structure changes in barnase on ligand binding reveal intermediate rate fluctuations, Biophys. J 97 (2009) 1482–1490. [PubMed: 19720037]

[76]. Kitahara R, Hata K, Li H, Williamson MP, and Akasaka K Pressure- induced chemical shifts as probes for conformational fluctuations in proteins, Prog. Nucl. Magn. Reson. Spectrosc 71 (2013) 35–58. [PubMed: 23611314]

[77]. La Penna G, Mori Y, Kitahara R, Akasaka K, and Okamoto Y Modeling (15)N NMR chemical shift changes in protein backbone with pressure, J. Chem. Phys 145 (2016) 085104. [PubMed: 27586953]

[78]. Li H, Yamada H, Akasaka K, and Gronenborn AM Pressure alters electronic orbital overlap in hydrogen bonds, J. Biomol. NMR 18 (2000) 207–216. [PubMed: 11142511]

[79]. Koehler J, Beck Erlach M, Crusca E, Kremer W, Munte CE, and Kalbitzer HR Pressure dependence of 15N chemical shifts in model peptides Ac-Gly-Gly- X-Ala-NH2, Materials 5 (2012) 1774–1786.

[80]. Erlach MB, Koehler J, Crusca E, Jr., Kremer W, Munte CE, and Kalbitzer HR Pressure dependence of backbone chemical shifts in the model peptides Ac- Gly-Gly-Xxx-Ala-NH2, J. Biomol. NMR 65 (2016) 65–77. [PubMed: 27335085]

[81]. Frach R, Kibies P, Bottcher S, Pongratz T, Strohfeldt S, Kurrmann S, Koehler J, Hofmann M, Kremer W, Kalbitzer HR, Reiser O, Horinek D, and Kast SM The chemical shift baseline for high-pressure NMR spectra of proteins, Angew. Chem. Int. Ed. Engl 55 (2016) 8757–8760. [PubMed: 27282319]

[82]. Munte CE, Beck-Erlach M, Kremer W, Koehler J, and Kalbitzer HR Distinct conformational states of the alzheimer b-amyloid peptide can be detected by high-pressure NMR spectroscopy, Angew. Chem. Int. Ed. Engl 52 (2013) 8943–8947. [PubMed: 23843225]

[83]. Akasaka K Probing conformational fluctuation of proteins by pressure perturbation, Chem. Rev 106 (2006) 1814–1835. [PubMed: 16683756]

[84]. Beck Erlach M, Koehler J, Moeser B, Horinek D, Kremer W, and Kalbitzer HR Relationship between nonlinear pressure-induced chemical shift changes and thermodynamic parameters, J. Phys. Chem. B 118 (2014) 5681–5690. [PubMed: 24798035]

[85]. Wand AJ and Nucci NV Reply to Kitahara and Mulder: An ensemble view of protein stability best explains pressure effects in a T4 lysozyme cavity mutant, Proc. Natl. Acad. Sci. USA 112 (2015) E924. [PubMed: 25630509]

[86]. Kitahara R and Mulder FA Is pressure-induced signal loss in NMR spectra for the Leu99Ala cavity mutant of T4 lysozyme due to unfolding?, Proc. Natl. Acad. Sci. USA 112 (2015) E923. [PubMed: 25630507]

[87]. Akasaka K, Li H, Yamada H, Li R, Thoresen T, and Woodward CK Pressure response of protein backbone structure. Pressure-induced amide 15N chemical shifts in BPTI., Protein Sci 8 (1999) 1946–1953. [PubMed: 10548039]

[88]. Louis JM and Roche J Evolution under drug pressure remodels the folding free-energy landscape of mature HIV-1 protease, J. Mol. Biol 428 (2016) 2780– 2792. [PubMed: 27170547]

[89]. Roche J, Louis JM, Grishaev A, Ying J, and Bax A Dissociation of the trimeric gp41 ectodomain at the lipid-water interface suggests an active role in HIV-1 Env-mediated membrane fusion, Proc. Natl. Acad. Sci. USA 111 (2014) 3425–3430. [PubMed: 24550514]

[90]. Kitahara R, Yokoyama S, and Akasaka K NMR snapshots of a fluctuating protein structure: ubiquitin at 30 bar-3 kbar, J. Mol. Biol 347 (2005) 277–285. [PubMed: 15740740]

[91]. Fu YN and Wand AJ Partial alignment and measurement of residual dipolar couplings of proteins under high hydrostatic pressure, J. Biomol. NMR 56 (2013) 353–357. [PubMed: 23807390]

[92]. Roche J, Louis JM, Bax A, and Best RB Pressure-induced structural transition of mature HIV-1 protease from a combined NMR/MD simulation approach, Proteins 83 (2015) 2117–2123. [PubMed: 26385843]

[93]. Sibille N, Dellarole M, Royer C, and Roumestand C Measuring residual dipolar couplings at high hydrostatic pressure: robustness of alignment media to high pressure, J. Biomol. NMR 58 (2014) 9–16. [PubMed: 24292655]

[94]. Lipari G and Szabo A Model-free approach to the interpretation of nuclear magnetic resonance relaxation in macromolecules. 1. Theory and range of validity, J. Am. Chem. Soc 104 (1982) 4546–4559.

[95]. Caro JA, Harpole KW, Kasinath V, Lim J, Granja J, Valentine KG, Sharp KA, and Wand AJ Entropy in molecular recognition by proteins, Proc. Natl. Acad. Sci. USA 114 (2017) 6563–6568. [PubMed: 28584100]

[96]. Wand AJ and Sharp KA Measuring entropy in molecular recognition by proteins, Annu. Rev. Biophys 47 (2018) 2.1–2.21.

[97]. Sareth S, Li H, Yamada H, Woodward CK, and Akasaka K Rapid internal dynamics of BPTI is insensitive to pressure 15N spin relaxation at 2 kbar, FEBS Lett 470 (2000) 11–14. [PubMed: 10722836]

[98]. Lee AL, Sharp KA, Kranz JK, Song X-J, and Wand AJ Temperature dependence of the internal dynamics of a calmodulin-peptide complex., Biochemistry 41 (2002) 13814–13825. [PubMed: 12427045]

[99]. Igumenova TI, Frederick KK, and Wand AJ Characterization of the fast dynamics of protein amino acid side chains using NMR relaxation in solution, Chem. Rev 106 (2006) 1672–1699. [PubMed: 16683749]

[100]. Wagner G Activation volumes for the rotational motion of interior aromatic rings in globular proteins determined by high resolution 1H NMR at variable pressure, FEBS Lett 112 (1980) 280–284. [PubMed: 6154600]

[101]. Li H, Yamada H, and Akasaka K Effect of rressure on the tertiary structure and dynamics of folded basic pancreatic trypsin inhibitor, Biophys. J 77 (1999) 2801–2812. [PubMed: 10545378]

[102]. Hattori M, Li H, Yamada H, Akasaka K, Hengstenberg W, Gronwald W, and Kalbitzer HR Infrequent cavity-forming fluctuations in HPr from Staphylococcus carnosus revealed by pressure- and temperature-dependent tyrosine ring flips, Protein Sci 13 (2004) 3104–3114. [PubMed: 15557257]

[103]. Weininger U, Modig K, and Akke M Ring flips revisited: C-13 relaxation dispersion measurements of aromatic side chain dynamics and activation barriers in basic pancreatic trypsin inhibitor, Biochemistry 53 (2014) 4519– 4525. [PubMed: 24983918]

[104]. Korzhnev DM, Bezsonova I, Evanics F, Taulier N, Zhou Z, Bai Y, Chalikian TV, Prosser RS, and Kay LE Probing the transition sate ensemble of a protein folding reaction by pressure-dependent NMR relaxation dispersion, J. Am. Chem. Soc 128 (2006) 5262–5269. [PubMed: 16608362]

[105]. Bezsonova I, Korzhnev DM, Prosser RS, Forman-kay JD, and Kay LE Hydration and packing along the folding pathway of SH3 domains by pressure-dependent NMR, Biochemistry 45 (2006)

[106]. Lassalle MW, Yamada H, Morii H, Ogata K, Sarai a., and Akasaka K Filling a cavity dramatically increases pressure stability of the c-Myb R2 subdomain, Proteins 45 (2001) 96–101. [PubMed: 11536365]

[107]. Kamatari YO, Smith LJ, Dobson CM, and Akasaka K Cavity hydration as a gateway to unfolding: an NMR study of hen lysozyme at high pressure and low temperature, Biophys. Chem 156 (2011) 24–30. [PubMed: 21367514]

[108]. Bai YW, Sosnick TR, Mayne L, and Englander SW Protein folding intermediates - Native state hydrogen exchange., Science 269 (1995) 192–197. [PubMed: 7618079]

[109]. Gledhill JM, Walters BT, and Wand AJ AMORE-HX: a multidimensional optimization of radial enhanced NMR-sampled hydrogen exchange, J. Biomol. NMR 45 (2009) 233–239. [PubMed: 19633974]

[110]. Otting G, Liepinsh E, and Wuthrich K Protein hydration in aqueous solution, Science 254 (1991) 974–980. [PubMed: 1948083]

[111]. Wand AJ, Ehrhardt MR, and Flynn PF High-resolution NMR of encapsulated proteins dissolved in low-viscosity fluids, Proc. Nat. Acad. Sci. USA 95 (1998) 15299–15302. [PubMed: 9860963]

[112]. Nucci NV, Valentine KG, and Wand AJ High-resolution NMR spectroscopy of encapsulated proteins dissolved in low-viscosity fluids, J. Magn. Reson 241 (2014) 137–147. [PubMed: 24656086]

[113]. Nucci NV, Pometun MS, and Wand AJ Site-resolved measurement of water-protein interactions by solution NMR, Nat Struct Mol Biol 18 (2011) 245– 249. [PubMed: 21196937]

[114]. Nucci NV, Pometun MS, and Wand AJ Mapping the hydration dynamics of ubiquitin, J Am Chem Soc 133 (2011) 12326–12329. [PubMed: 21761828]

[115]. Wirth AJ, Liu Y, Prigozhin MB, Schulten K, and Gruebele M Comparing fast pressure jump and temperature jump protein folding experiments and simulations, J. Am. Chem. Soc 137 (2015) 7152–7159. [PubMed: 25988868]

[116]. Prigozhin MB, Liu Y, Wirth AJ, Kapoor S, Winter R, Schulten K, and Gruebele M Misplaced helix slows down ultrafast pressure-jump protein folding, Proc. Natl. Acad. Sci. USA 110 (2013) 8087–8092. [PubMed: 23620522]

[117]. Alderson TR, Charlier C, Torchia DA, Anfinrud P, and Bax A Monitoring Hydrogen Exchange During Protein Folding by Fast Pressure Jump NMR Spectroscopy, J Am Chem Soc 139 (2017) 11036–11039. [PubMed: 28766333]

[118]. Fuentes EJ and Wand AJ Local stability and dynamics of apocytochrome b(562) examined by the dependence of hydrogen exchange on hydrostatic pressure, Biochemistry 37 (1998) 9877–9883. [PubMed: 9665691]

- High-pressure NMR is now routinely accessible
- Pressure provides access to fundamental thermodynamics
- Pressure perturbation is complementary to temperature and chemical perturbation
- Novel insights into protein dynamics and hydration are possible

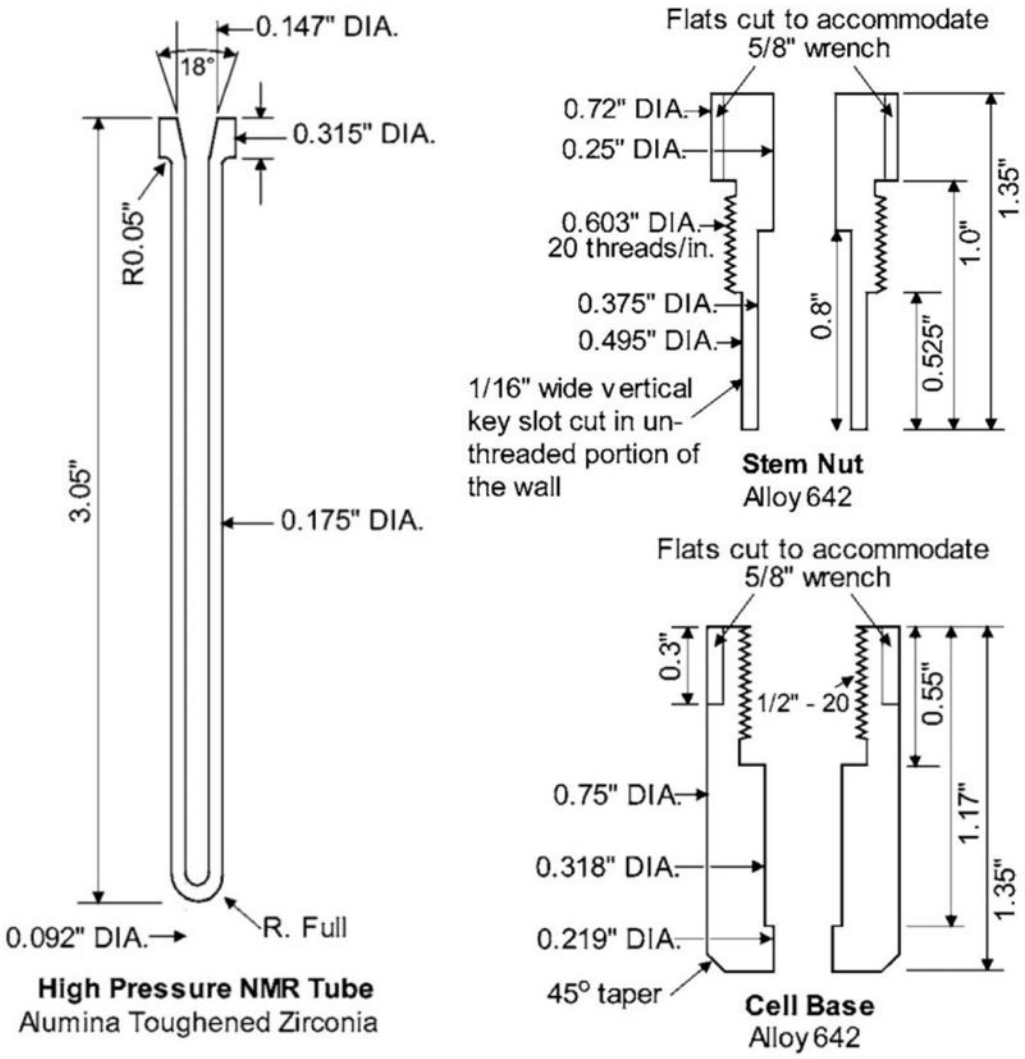

Figure 1.

High-pressure NMR cell and design. A two-component valve system (right) holds and seals the alumina-toughened zirconia NMR tube (left). Reprinted from [53] with permission of AIP Publishing.

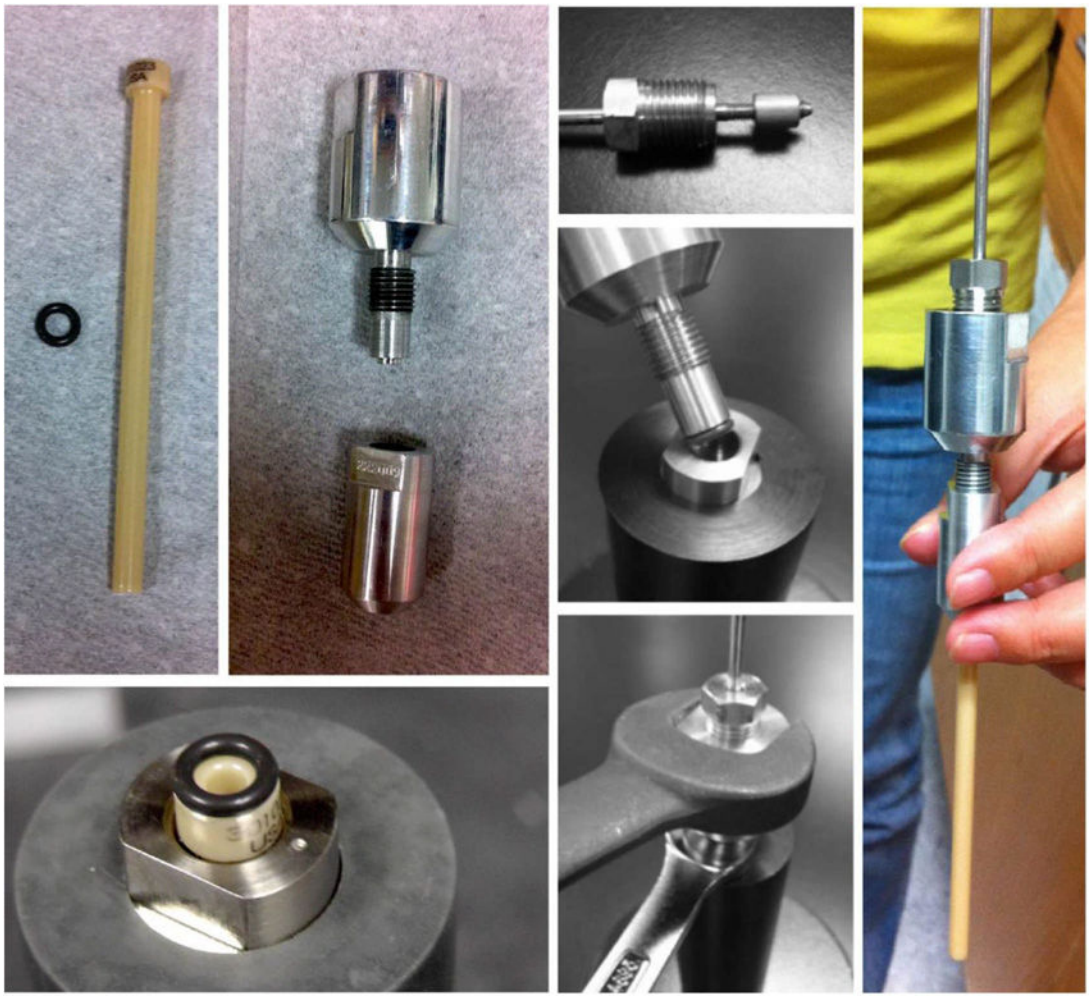

Figure 2.

Assembly of NMR cell. The NMR tube and its o-ring are seated in the lower half of the metal valve and aligned using a setup tool (left). The upper half of the cell is then screwed on and iterative cycles of tightening and aligning are performed using a torque wrench set to 130 lb. in. (middle). The sealed pressure valve-NMR tube assembly is connected to a pressure generator via a tether that is screwed on to the top of the cell (right). Some photos courtesy of Daedalus Innovations LLC.

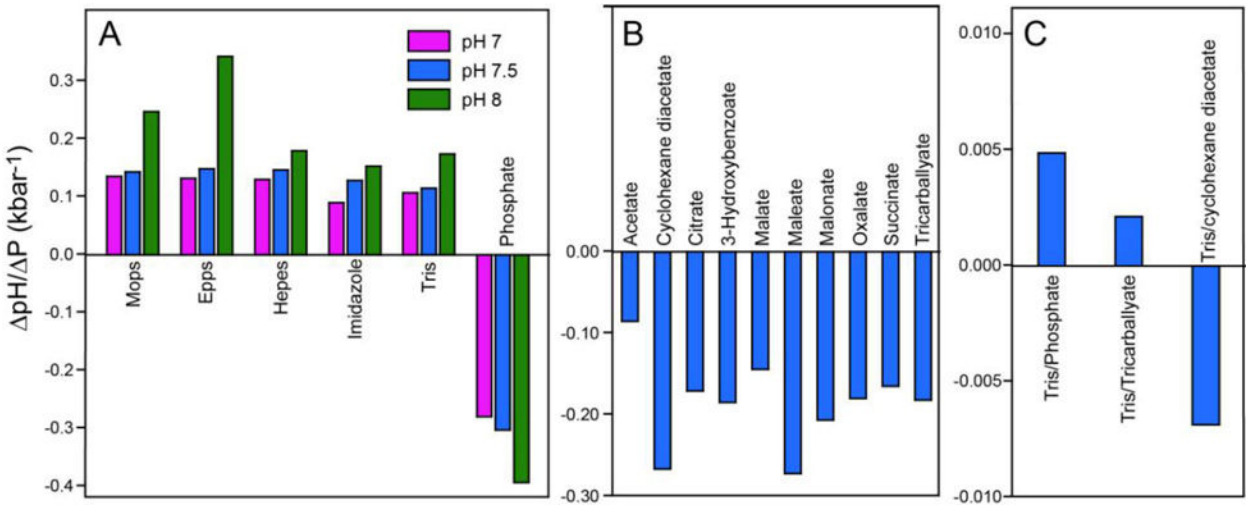

Figure 3.

Pressure-sensitivity of buffers. Common cationic (A) and anionic (B) buffers can have large variations in pKa with pressure that will result in changes in pH with pressure. Unwanted contributions to ΔV and changes in pH due to buffers can be largely avoided by appropriate combinations of buffer components (C). Redrawn from Quinlan and Reinhart [67].

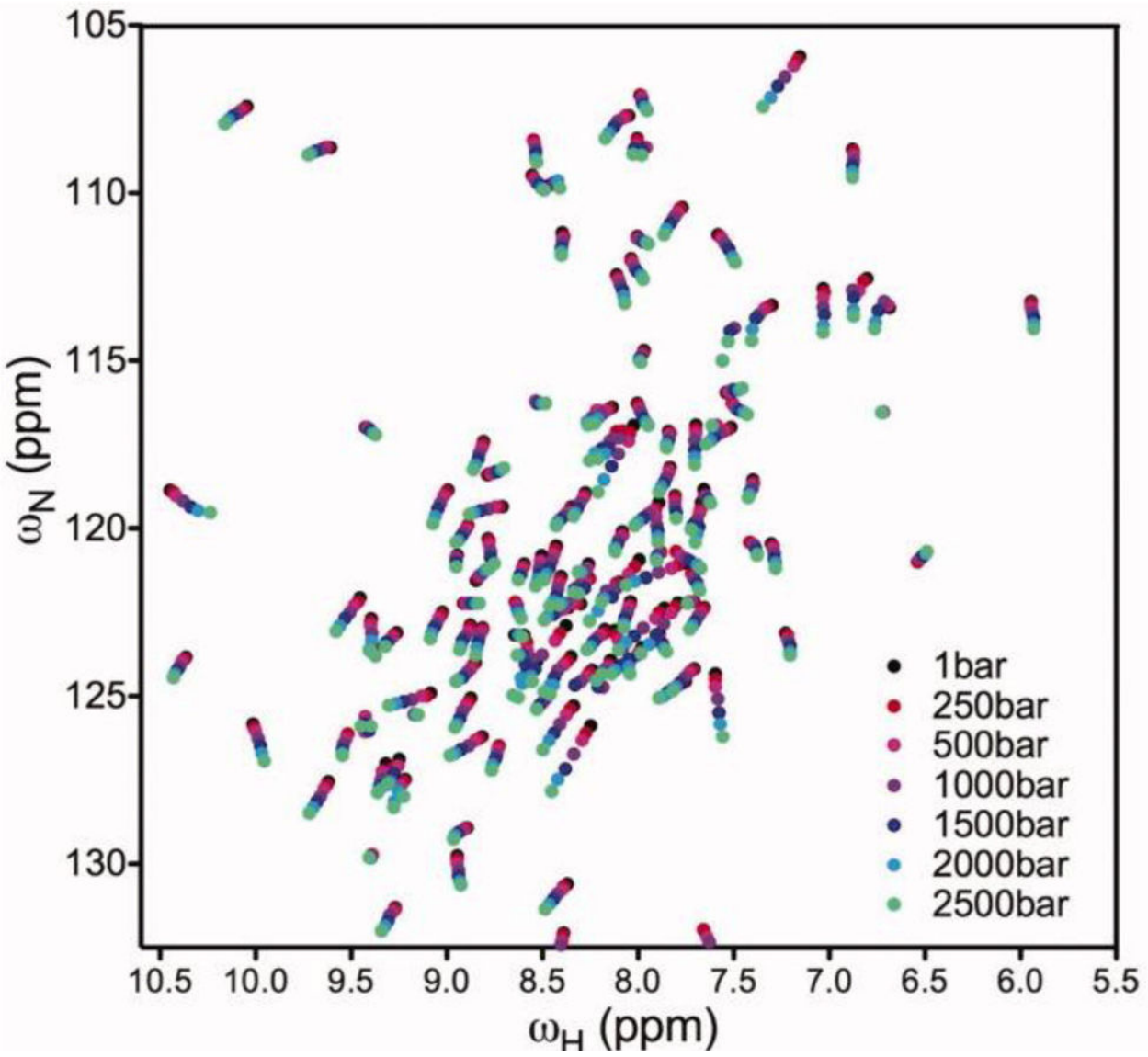

Figure 4.

Linear and non-linear responses of chemical shifts to pressure. Amide resonances of SNase are followed as a function of pressure to monitor the response of the native state and characterize its mechanisms of compression. Arrows indicate some examples of resonances with non-linear responses of their chemical shifts to pressure. Reprinted from Roche et al [11] with permission of Wiley Publishing.

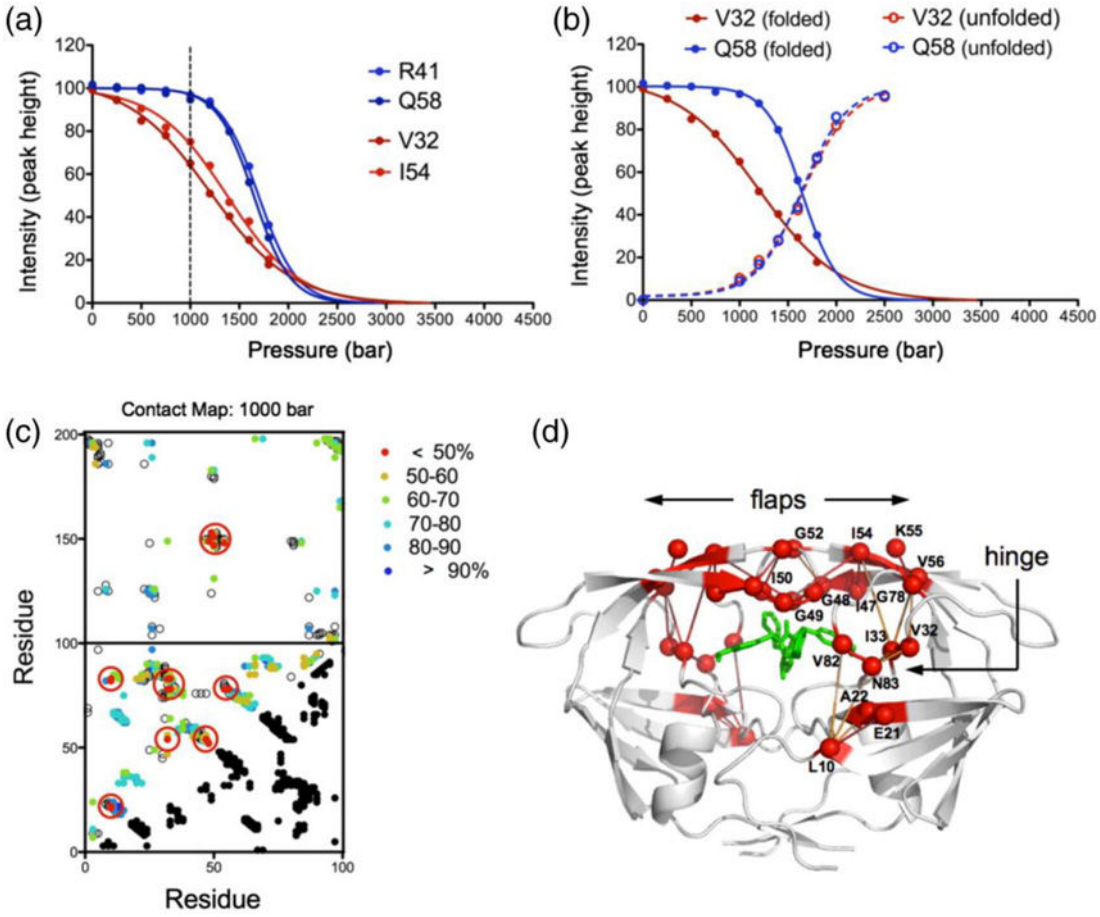

Figure 5.

Cooperative and non-cooperative transitions observed for folded and unfolded states. By monitoring resonances from both the folded (a, solid lines in b) and unfolded (dashed lines in b) states, it is possible to identify regions within the protein that undergo more complex exchange processes and have low probability of maintaining native contacts at high pressure (c). These regions coincide with the so-called flap and hinge domains of HIV-1 protease, involved in the binding of inhibitor (d, highlighted in red). Reprinted from Louis and Roche [88] with permission from Elsevier Publishing.

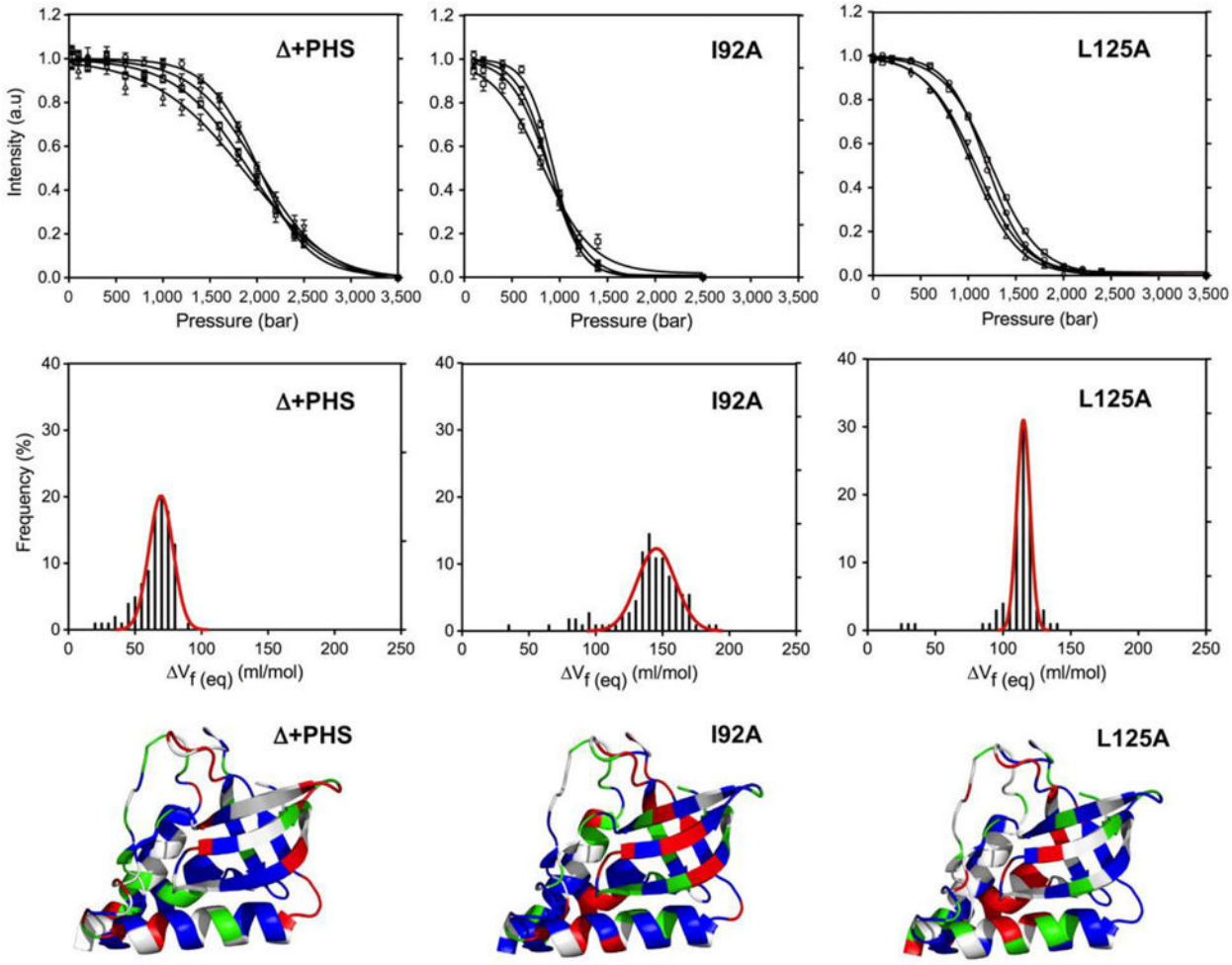

Figure 6.

Unfolding profiles of the NH resonances in SNase and its variants with engineered cavities. Amide resonance intensity is followed as a function of pressure (top), revealing a broad range of ΔV values (middle). The distribution of ΔV values , their mean value, and how they map onto the crystal structure are highly sensitive to the presence and location of artificial cavities (bottom, with above, within and below the standard deviation colored red, blue and green). Reprinted from Roche et al [31].

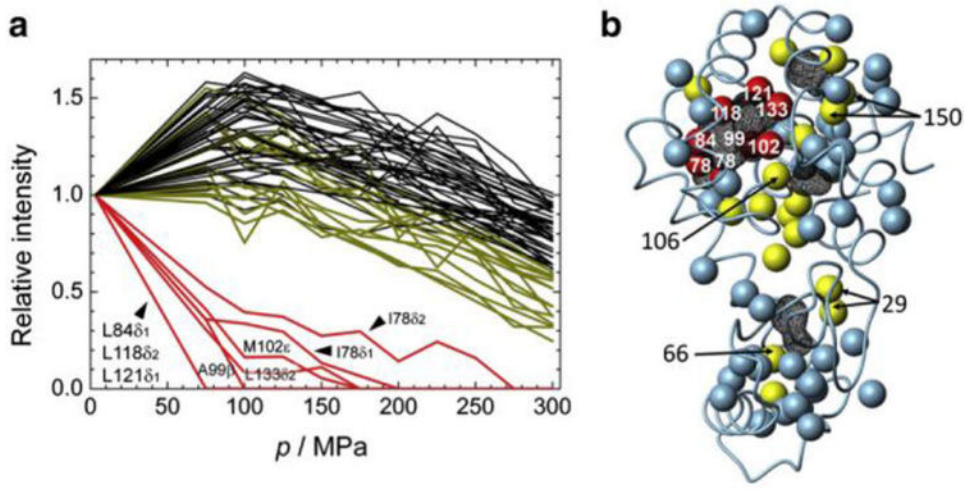

Figure 7.

Highly heterogeneous response of methyl resonances due to the presence of an artificial cavity. The intensity of methyl crosspeaks reveals a starkly different behavior for methyls adjacent to the engineered cavity (a, red lines, and b, red spheres), which disappear at much lower pressures than the rest of the pressure sensitive resonances (black and yellow lines). Reprinted with permission from Maeno et al [42].

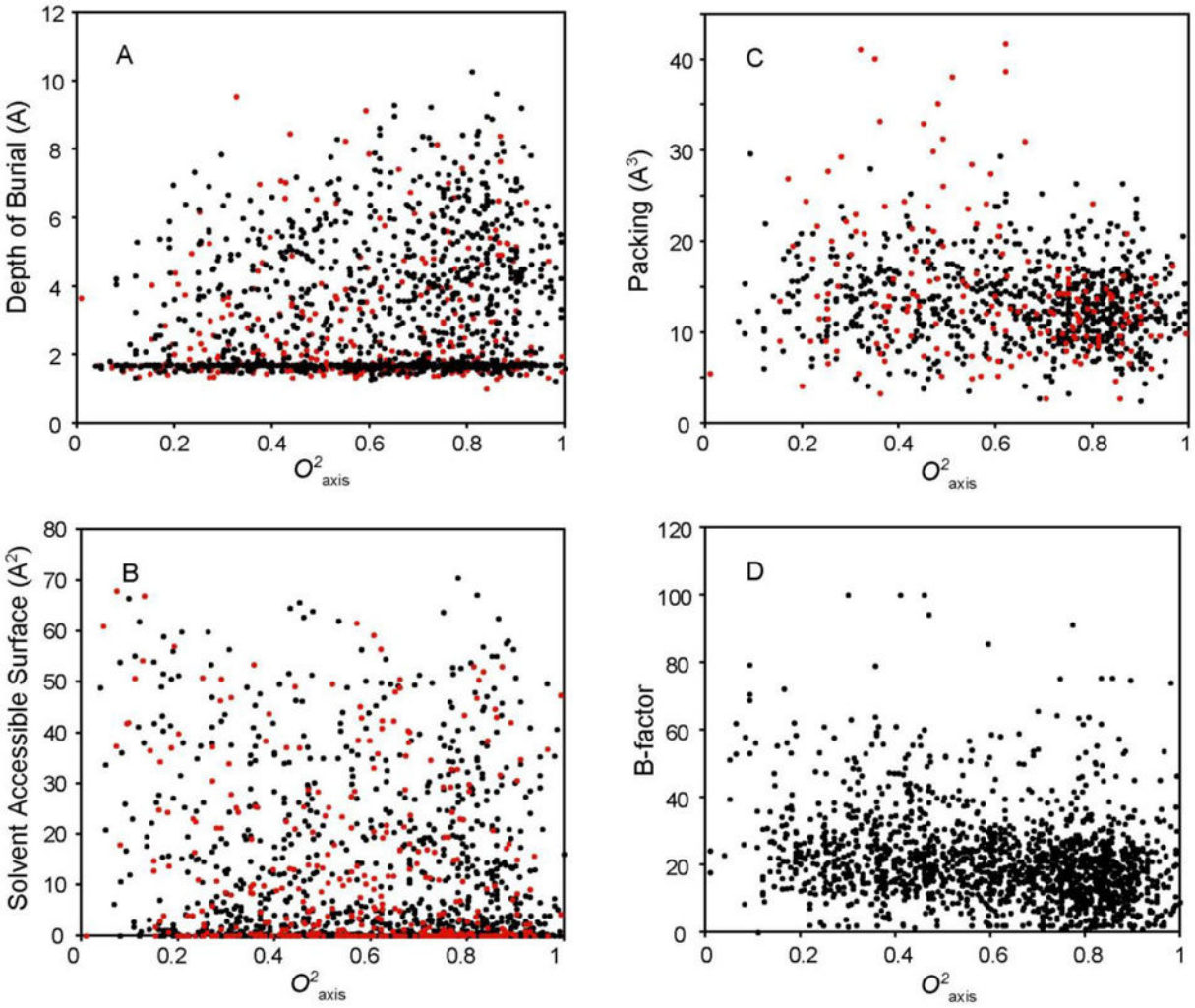

Figure 8.

Unclear physical origins of side chain dynamics. Order parameters (O^2_{axis}) determined by deuterium relaxation are plotted against several structural parameters obtained from structures determined by crystallography (black symbols) or by NMR spectroscopy (red symbols). The plots make it apparent that no clear correlations exist. Pressure offers a new avenue to better understand the determinants of protein fluctuations. Reprinted with permission from Igumenova et al . Copyright (2006) American Chemical Society.

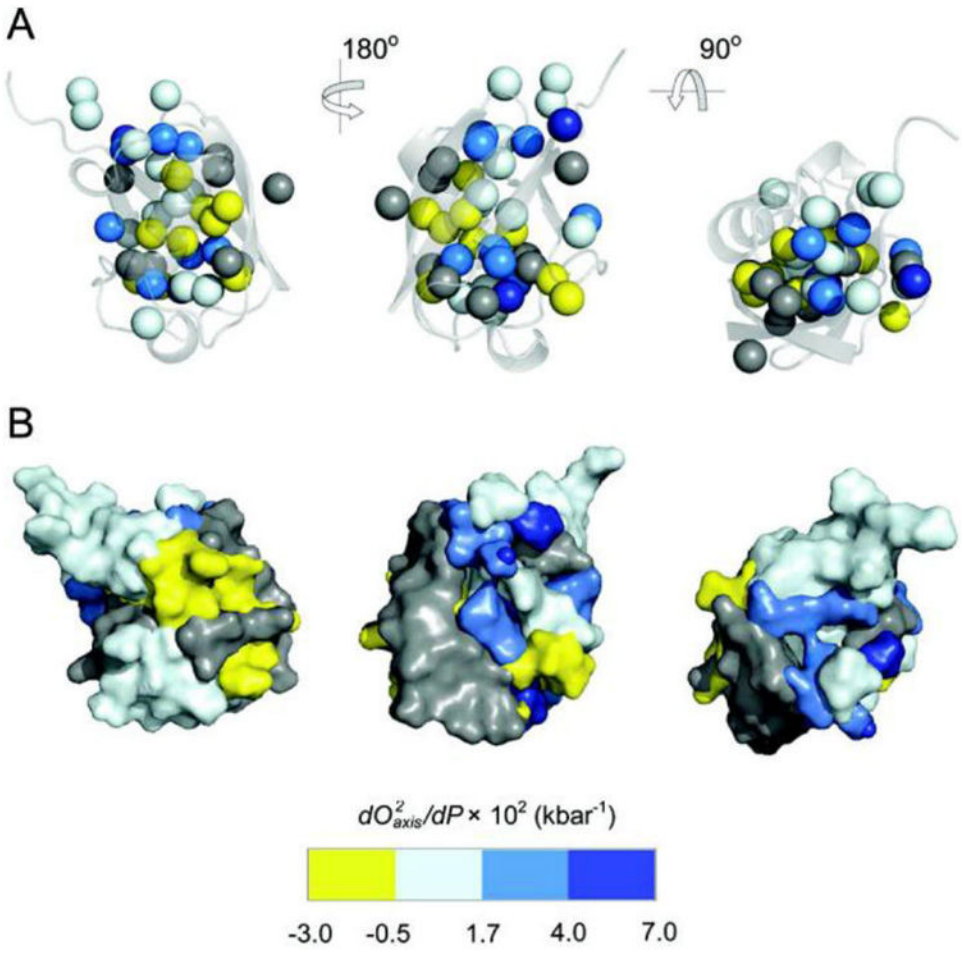

Figure 9.

Pressure sensitivity of side chain dynamics. Deuterium methyl relaxation was used to monitor the response of side chain motion in ubiquitin to pressure. Structural clustering is observed for the linear component of both positive and negative responses to pressure (regions in blue and yellow, respectively). In addition to shedding light on physical mechanisms of compression, these data suggest weak and rather localized coupling of internal side chain motion. Reprinted with permission from Fu et al [43]. Copyright (2012) American Chemical Society.

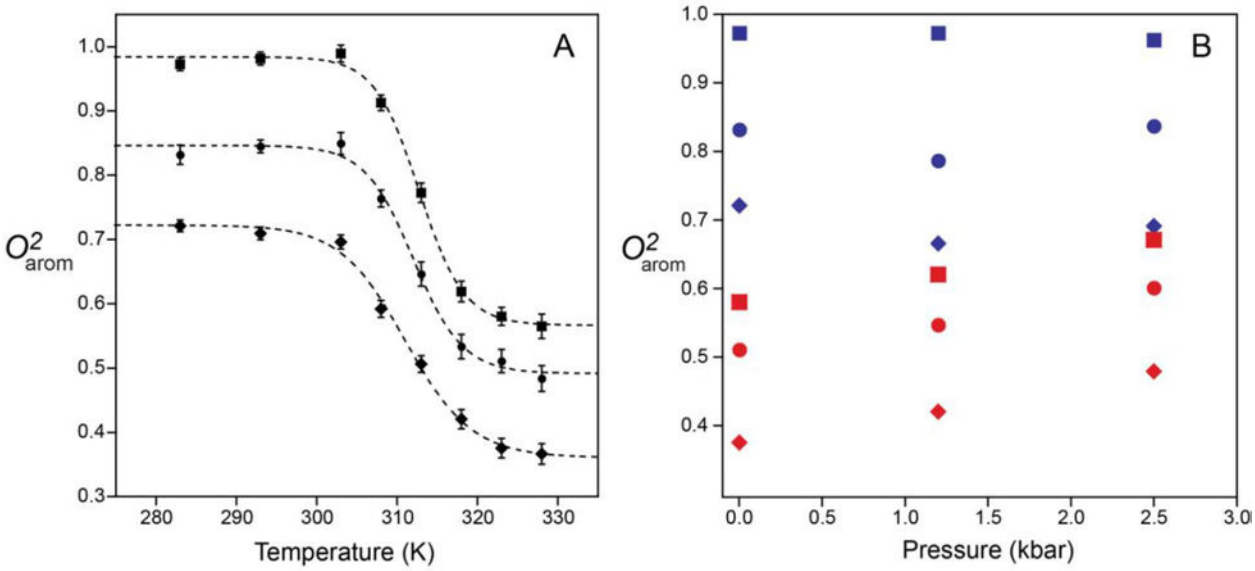

Figure 10.

Aromatic side chain motion in ubiquitin made evident by temperature (A) and pressure (B) perturbations. Ring flip motions become evident at higher temperatures, where they enter the fast NMR timescale. In this regime the pressure dependence of aromatics (B, red squares) and of methyl side chains (Figure 9, blue sites) have similar pressure dependencies, indicative of a highly mobile interior of the protein. Reprinted from Kasinath et al [44] with permission from Wiley Publishing.

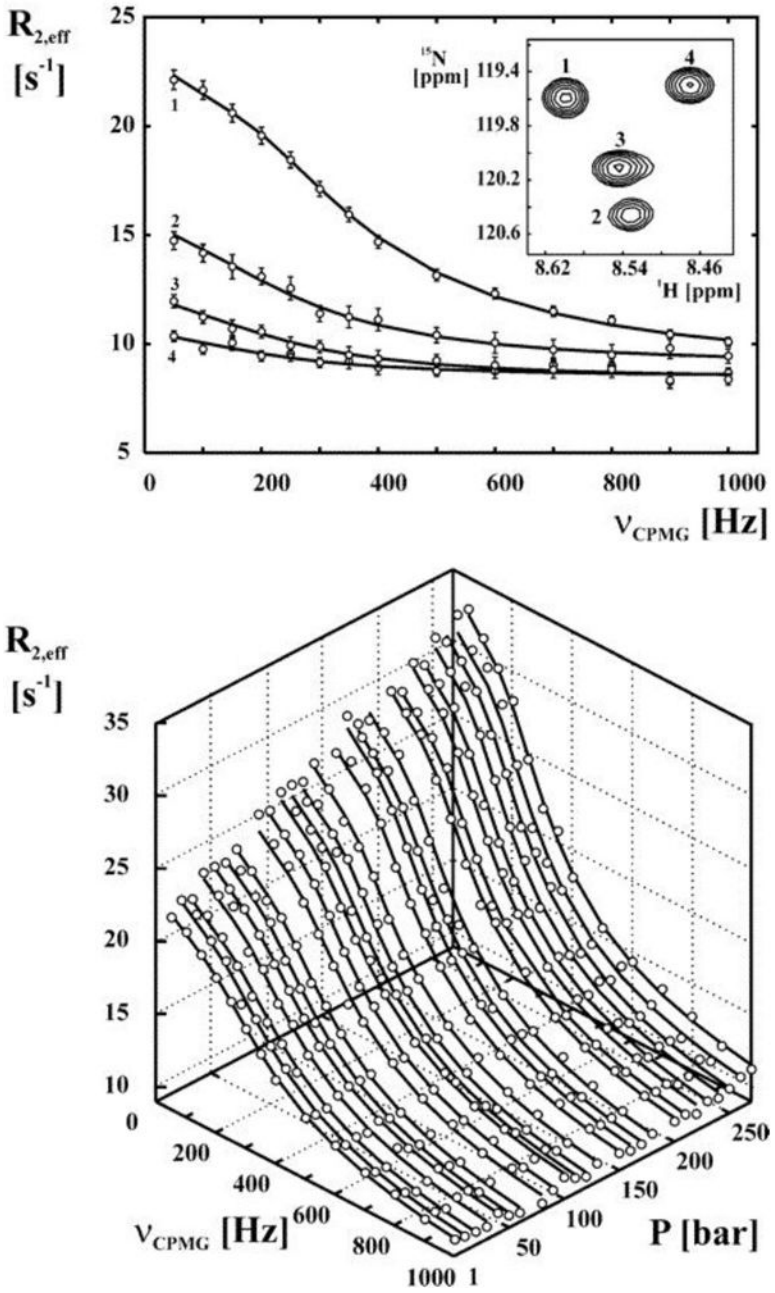

Figure 11.

Transition state thermodynamics accessed by low pressures. Relaxation dispersion is used to access intermediate timescale exchange between folded and unfolded protein (top panel). The pressure sensitivity of the dispersion (bottom panel) provides access to transition state volumes and suggested a more compressible transition state ensemble relative to the native ensemble. Reprinted form Korzhnev et al with permission. Copyright (2006) American Chemical Society.

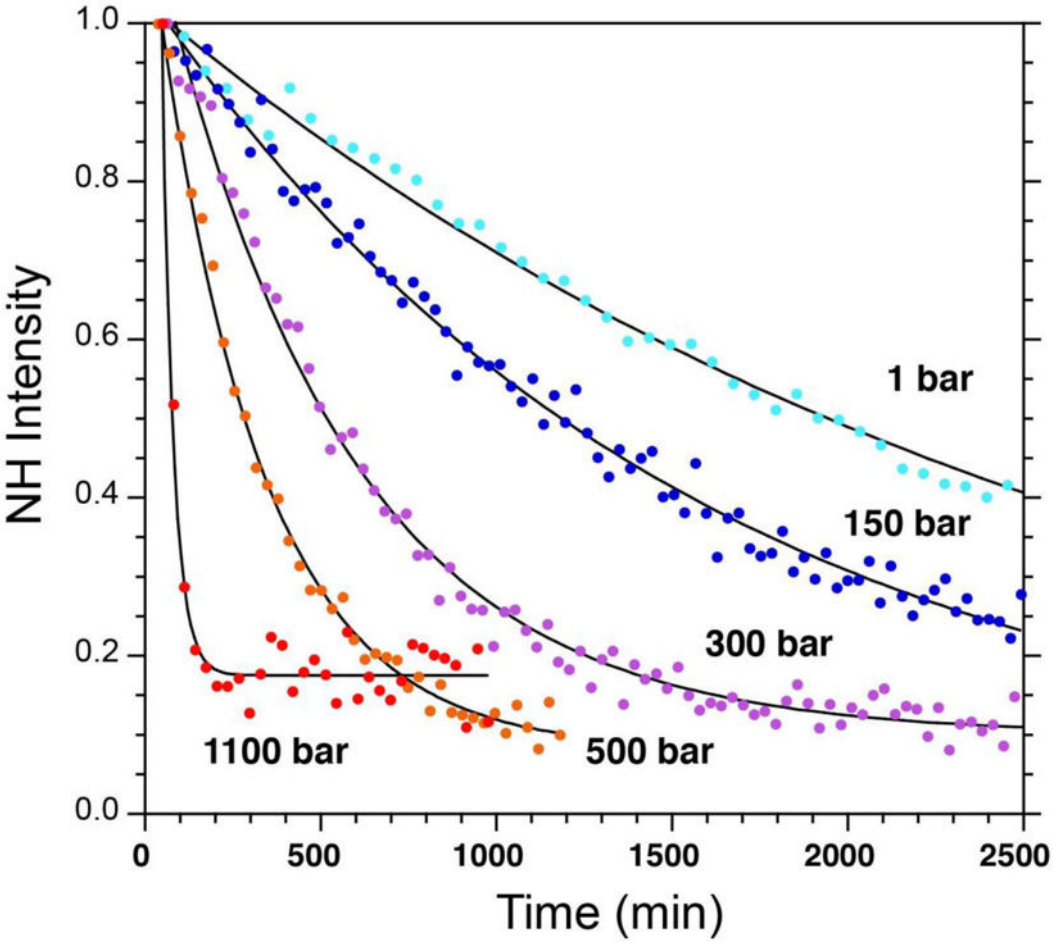

Figure 12.

Local volume changes and thermodynamic stability of proteins revealed by hydrogen exchange as a function of pressure. Amide resonance intensity is monitored at various pressures as it decays due to exchange with deuterium. At higher pressures, the protein stability decreases, leading to increased fluctuations and faster hydrogen exchange (e.g., red curve). Native-state hydrogen exchange can be utilized to uncover the cooperative substructure of proteins [108]. Pressure is a useful thermodynamic perturbation in this regard and offers a complementary view of native-state HX carried out using the more traditional chemical perturbation. Redrawn from Fuentes and Wand [118]. Copyright (1998) American Chemical Society.

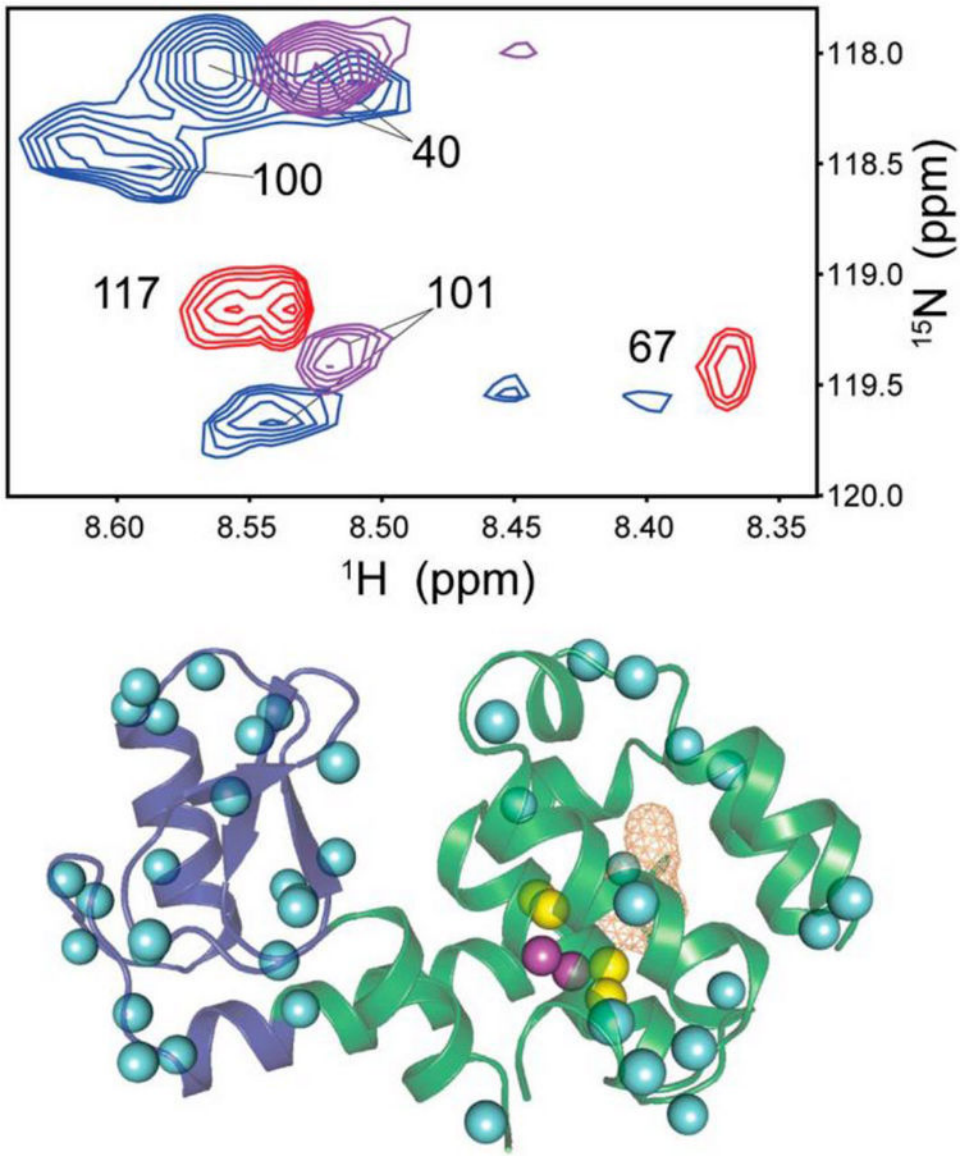

Figure 13.

Pressure permits exploration of protein solvation thermodynamics. Encapsulation of the T4 lysozyme in the aqueous nanoscale core of a reverse micelle enables the use of ^{1}H-^{1}H NOE/ROE ratios [110] to examine hydration of the hydrophobic cavity generated by the L99A mutation. The confined space effect of encapsulation suppresses the pressure-induced unfolding transition and allows observation of the filling of the cavity with water at elevated pressures. New resonances that result from long-lived interactions with water appear as pressure is increased from 1 bar (red) to 1 kbar (purple) to 2 kbar (blue) (top). Amides of residues 100 and 101 report on increased hydration due to pressure and are shown as magenta spheres (bottom). These coincide with where the artificial cavity is (orange mesh). Not all amides adjacent to the cavity report on increased hydration (yellow spheres). Reprinted from Nucci et al [13].

Table 1.

Composition of pressure insensitive buffers.[a]

Components	pH	Tris base (ratio)
Tris/Tricarballylate	7.0	0.448
	7.5	2.063
	8.0	7.757
Tris/phosphate	7.0	0.119
	7.5	0.416
	8.0	2.997
Tris/CDA	7.0	0.104
	7.5	0.314
	8.0	1.698

[a]Values determined for a 100 mM buffering capacity.